Title
Gas Tungsten Arc Welding of Aluminum Alloys with Nanocomposite 4943 Filler Material

Author
Bethea, John Franklin

Publication Date
2019

Peer reviewed|Thesis/dissertation

UNIVERSITY OF CALIFORNIA

Los Angeles

Gas Tungsten Arc Welding of Aluminum Alloys with Nanocomposite 4943 Filler Material

A thesis submitted in partial satisfaction of the requirements for the degree Master of Science in Mechanical Engineering

by

John Franklin Bethea

2019

ABSTRACT OF THE THESIS

Gas Tungsten Arc Welding of Aluminum Alloys

with Nanocomposite 4943 Filler Material

by

John Franklin Bethea

Master of Science in Mechanical Engineering

University of California, Los Angeles, 2019

Professor Xiaochun Li, Chair

Aluminum alloy 4943, specifically developed for arc welding, offers higher tensile and yield strength than AA 4043 and AA 4643 while maintaining weldability characteristics such as fluidity, shrinkage, solidification range, and low weld cracking sensitivity[1]. Thus, it has become a preferred filler material option for high quality, repeatable welds, especially for 6xxx series aluminum. However, the strength and applicability of aluminum alloy welded joints with AA 4943 filler material remains limited despite excellent weldability. Previous studies[2] have shown the promise of introducing ceramic nanoparticles into the aluminum alloy filler material to enhance mechanical properties and avoid problems typically associated with aluminum welding, such as solidification cracking. This idea has been extrapolated to AA 4943, which can be modified to produce welds with nanocomposite filler material. Any perceived benefits would have implications for many industries, in particular bicycle manufacturing which commonly uses AA 6061 for frames.

By introducing TiB_2 nanoparticles into AA 4943 to produce welds of popular aluminum alloys through gas tungsten arc welding (GTAW), the effects of this nanocomposite

filler were studied through characterization methods including microhardness testing, microstructure determination, and tensile testing. Little to no enhancements to mechanical properties were observed for welds with AA 4943 TiB_2 nanocomposite filler when compared to welds with AA 4943 reference filler. Large clusters of TiB_2 nanoparticles were observed in the secondary phase of the nanocomposite AA 4943 following casting and also observed in the as-welded samples in the weld zone. These clusters may be hindering ductility and providing a brittle fracture surface, lowering ultimate tensile strength of the samples and offering no grain size refinements. Additional manufacturing methods for the nanocomposite filler, such as extrusion, may offer a solution to the TiB_2 clustering effect and superior nanoparticle distribution.

The thesis of John Franklin Bethea is approved.

Yongjie Hu

Yongho Sungtaek Ju

Xiaochun Li, Committee Chair

University of California, Los Angeles

2019

Tables and Figures

Acknowledgements

I would like to thank Professor Xiaochun Li for giving me the opportunity to perform research in his lab on the frontier of nanotech metallurgy. From classes to research, I learned an immense amount from Professor Li during my Master's studies and I greatly appreciate his wisdom and inspiration for making scientific discoveries.

I would also like to thank Maximilian Sokoluk, who was a true guiding force during my research and served as an incredible mentor. Max taught me the entire research process for my thesis, from welding to characterization, and provided invaluable feedback on my results. Thank you Max!

I. Introduction/Motivation

Aluminum alloys are a popular choice for transportation applications, where lightweight and corrosion resistant materials are needed to maximize fuel efficiency and protect against outdoor elements; they have a very low density compared to steel and with proper treatment can resist the oxidation process that affects steel including corrosion by water, salt, and other factors[3]. Previous studies have shown that a 10% weight reduction results in a 6-8% increase in fuel economy for automobiles[4]. This can be extended to electric bicycles, where saving on battery life is critical and a reduction in weight of the bike can make a dramatic impact. Weldability of these alloys is of central importance in selecting appropriate materials for structural applications.

Heat-treatable aluminum alloys, such as 2xxx, 6xxx, and 7xxx series alloys, have become very popular choices due to their superior strength-to-weight ratio. In the cycling industry, bicycle frames are typically made from 6061 aluminum as it is easy to heat treat, easy to weld, resistant to corrosion and fatiguing, and easy to hydroform. Aluminum alloy (AA) 4043 filler is the most popular filler alloy for general purpose aluminum welding due to its excellent corrosion characteristics, low melting temperature, low shrinkage rate, higher fluidity, and low hot cracking sensitivity. AA 4943, which was recently developed for welding filler applications, has become a very popular choice for aluminum welding filler material as it retains advantages of AA 4043 while also exhibiting higher tensile, yield, and shear strength. AA 4943 is also heat treatable and exhibits improved strength in post-weld heat treated and artificially aged condition when compared to heat-treatable AA 4643, which has been generally used to weld 6xxx series base metals that are post-weld heat treated[1]. Despite these advantages, AA 4943 is not typically used to weld AA 2024, AA 5083 with greater than 2.5% magnesium, or AA 7075. In addition, AA 4943 shows less strength characteristics than another commonly used filler material, AA 5356.

Previous studies have shown that through the addition of nanomaterial to the welding filler material, mechanical properties including tensile strength can be enhanced and adverse affects of aluminum welding, such as hot cracking, can be prevented[2]. This thesis seeks to study the strength characteristics and applicability of aluminum alloy welds with AA 4943 filler material through the addition of ceramic nanoparticles in the 4943 alloy, in particular titanium diboride (TiB_2). Based on the welds of a variety of different aluminum alloy base materials, the effect of nanocomposite 4943 on overall weldability of aluminum alloys can be examined. Popular aluminum alloy base materials were selected for this study, including AA 2024, AA 5083, AA 6061, and AA 7075. The mechanical properties of these alloys can be seen below in Table 1.

Table 1 Mechanical Properties of Aluminum Alloys

Aluminum Alloy	Density (g/cm^3)	Tensile Strength (MPa)	Specific strength ($Pa \cdot m^3/kg$)
2024-T3[5]	2.78	485	175
5083-H116[6]	2.66	317	119
6061-T6[5]	2.7	310	115
7075-T6[5]	2.81	572	204

II. Literature Review

Section 2.1 Arc welding of aluminum alloys

Fusion welding and solid state welding, or arc welding and friction stir welding (FSW), respectively, are two different methods of joining aluminum alloys. FSW has shown promise as a technique for welding previously unweldable alloys such as AA 7075; however, it is fully mechanized and cannot be used for complicated weld shapes with access restrictions[2]. Thus, arc welding is the preferred method for joining aluminum alloys in complex structures; however, this method experiences problems from the massive heat input and phase transitions.

Two popular arc welding methods for joining high strength aluminum alloys are gas tungsten arc welding (GTAW) and gas metal arc welding (GMAW)[7]. GTAW is also referred to as tungsten inert gas (TIG) welding, and GMAW is also referred to as metal inert gas (MIG) welding. The primary difference between these two processes is that GTAW uses a non-consumable tungsten electrode, while GMAW uses a consumable electrode. These two processes can be further broken down into subcategories of direct current (DC) arc welding and alternating current (AC) arc welding. AC welding is typically used for fusion welding of aluminum alloys as it supports welding at a higher temperature; when the AC switches to positive, it helps to remove the oxide film on the surface of aluminum and cleans the surface. AC welding also allows for deeper penetration into aluminum plates[8].

Many arc manipulation techniques exist to enhance the properties of aluminum welds, giving the welder superior control over the quality of the weld. Some of these techniques include arc oscillation, which can be used to mitigate hot cracking[9]. However, aluminum alloys remain susceptible to cracking and reductions in strength during the arc welding process. Problems associated with welding of aluminum alloys are discussed in depth below in Section 2.3.

Section 2.1.1 Gas tungsten arc welding (GTAW) of aluminum alloys

GTAW is a process that melts and joins metals by heating them with an arc formed between a non-consumable tungsten electrode and metals. Argon is used to provide a shield for the arc and the molten weld pool. This process welds most metals and metal alloys, including aluminum, magnesium, copper, brass, bronze, steels, nickel, and titanium[3]. Most precision parts are gas tungsten arc welded, including batteries, pacemakers, and medical components. An electrical arc is formed between the tungsten electrode and part to be welded using a high voltage to break down the insulating gas between the electrode and the part. Current is transferred through the electrode to create an electrode arc. The metal to be welded is melted by the intense heat of the arc; the argon provides protection for the tungsten electrode and the molten material from oxidization as well as providing a conducting path for the arc current.

Welding parameters are of most importance during this process as they directly affect the weld quality. These parameters include current, frequency, voltage, arc length, welding gun speed, welding gun position, shielding gas, and heat input[3]. Alternating current is best adapted for welding aluminum alloys as it allows for balancing of electrode heating and work-piece cleaning effects. The current alternates at a set frequency with no control over time or independent amplitude. Arc current corresponds to the amount of heat the arc produces from electricity.

Frequency directly affects the stability and directionality of the arc; a greater frequency corresponds to greater directionality, deeper penetration, less porosity in the weld metal, and greater welding speed. Arc length is the distance between the electrode tip and the workpiece, and usually ranges from 2 to 5 mm[10]. Successful welding depends on control of both arc current and arc length. If arc length increases, voltage to maintain the arc must also increase; however, heat input to the work piece decreases. The welding gun speed does not affect weld pool formation, only the volume of melted material; this value usually ranges from

100 to 500 mm/min depending on the current, material type, and plate thickness[3]. Electrode angles vary between 30° and 120°; angles between 60° and 120° maintain tip shape and give an adequate penetration depth-to-width ratio.

There are there main zones in a gas tungsten arc welded joint: the weld zone, heat affected zone (HAZ), and base metal[11]. The HAZ includes two subzones, one near the weld pool which experiences solution temperature, and one toward the base metal which is exposed to temperatures below the solution temperature and experiences overaging. Behind the subzone experiencing partial melting is completely solidified material called the partially melted zone (PMZ)[12]. A schematic showing these different areas of the weld can be seen below in Figure 2.1.1.

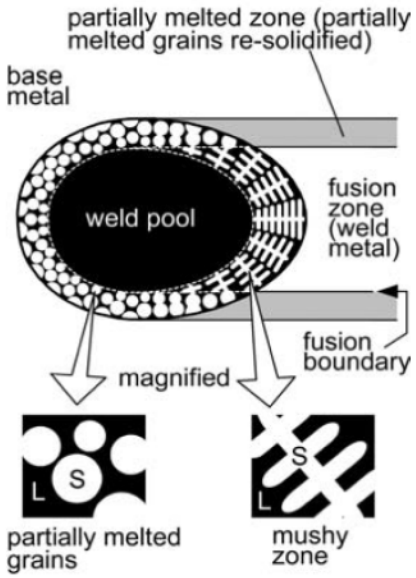

Figure 2.1.1 Semisolid materials around weld pool of alloy during welding[12]

Heat input is very important during the welding process as the thermal profile in the area near the weld has a significant impact on the formation of the HAZ, its microstructure and mechanical properties including joint strength. Too high of a heat input results in a decrease of the ultimate tensile strength in the welded joint. Microhardness also decreases rapidly with an

increase in heat input; an increase in the width of the HAZ and grain coarsening also occur with an increase in heat. Tensile fracture tends to occur in the HAZ with its lower microhardness due to grain coarsening from heat input. However, too low heat input results in pores and partial penetration; high heat input deepens weld penetration, increases welding speeds, and gives better weld quality while also decreasing weld strength of aluminum alloys.

Butt joints are typically used for plates of thickness 3 mm; penetration can be achieved at higher thickness by leaving a small gap, or root gap, between the edges to be joined. A backing bar or strip is used to support the root pass where control of the weld bead is difficult on the backside of the butt joint. This concept is shown below in Figure 2.1.2.

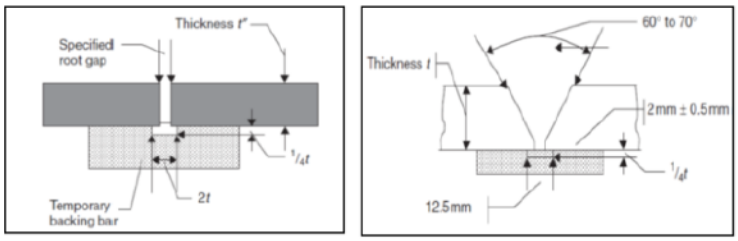

Figure 2.1.2 Butt Joint and Backing Bar[3]

Section 2.2 Filler material for GTAW

Filler materials are selected for aluminum welding based on similarity in alloying elements to the base material; in addition, characteristics in the liquid state are important to prevent cracking and properly disperse and fuse with the base material. For Al-Mg-Si alloys, a suitable choice of filler metal can enhance the strength of the fusion zone and HAZ[13]. The most popular, general purpose welding filler wires include AA 4043 and AA 5356, which were specifically designed as welding filler material. AA 4043 contains 5% silicon while AA 5356 contains 5% magnesium. AA 5356 is the preferred material when welding AA 6061 base material, as it is generally stronger and more ductile[14]; however, the silicon in AA 4043 allows it to flow better, have more crack resistance, and better weldability. AA 4943 serves as a kind of

hybrid of these two filler metal alloys, with the advantages of AA 4043 and an increase in strength and ductility. AA 4943 is currently suitable for all applications using 4043 — including 1xxx, 3xxx, 4xxx, and 6xxx base alloys; however, it is not recommended for 5xxx series alloys with above 2.5% magnesium, as coarse Mg_2Si may form and have a detrimental impact on joint strength and ductility.

AA 4943 was designed with magnesium as a strengthening element, which alloys it to not be solely dependent on base metal dilution diffusion. Magnesium combines with the available silicon to form Mg_2Si, an effective strengthening phase. Magnesium addition is set from 0.1% to 0.5% to achieve a specific amount of Mg_2Si precipitation while avoiding the crack sensitivity peak of 1% Mg_2Si[1]. Silicon is kept at 5.0-6.0% to maintain free silicon of AA 4043, which is essential for fluidity characteristics and resistance to hot cracking during solidification. Silicon also allows for greater fracture toughness and fatigue performance.

Section 2.3 Problems associated with welding aluminum alloys

Welding of aluminum is "general considered difficult due to high thermal conductivity, electrical conductivity, high thermal expansion coefficient, refractory aluminum oxide formation tendency, and low stiffness"[15]. This results in welding limitations including oxide removal and reduced strength in the weld and heat affected zone (HAZ), which determines the usability and quality of the welds[13]. In addition, hydrogen and other gases show high solubility in the molten state[3], causing porosity in the weld bead.

The main problems that occur when welding high strength aluminum alloys such as 7075 include porosity, oxide film removal during welding, hot cracking, stress corrosion cracking (SCC), and strength loss due to welding[3]. Hot cracking usually occurs in the fusion zone during solidification, or in the HAZs if some of the grains are partially melted during welding; hot cracking in HAZs is typically called liquation cracking. This cracking occurs during the final

stages of solidification due to small amounts of segregate-rich low melting point liquid separating solid grains and inducing stresses across adjacent grains. Cracking can be eliminated by several methods, including the use of small additions of elements to produce a small grain size and using a filler metal with a melting point close to that of the parent metal. Small weld beads generally have better properties and a higher resistance to hot cracking than large weld beads.

Stress corrosion cracking (SCC) occurs due to susceptible microstructures, corrosive environments, and tensile stresses[3]. 7xxx series alloys are more susceptible to SCC than 5xxx series alloys, particularly in the short-transverse (i.e. thickness) direction. Hydrogen-induced cracking is the main mechanism for SCC in 7xxx and 5xxx series alloys; heat treatment and tempering after welding can be used to minimize corrosion, including a retrogression and reaging (RRA) process[13]. This process allows for the disappearance of quenched-in dislocations adjacent to grain boundaries, which are susceptible to stress corrosion. Post-weld treatments are discussed in detail below in section 2.3.3.

There may be a substantial loss of strength in the HAZ; in cold worked alloys due to recrystallization and in heat-treated alloys due to dissolution of precipitates in 2xxx series and coarsening or over aging of precipitates in 6xxx and 7xxx series alloys. Loss of alloying elements from the weld pool may also occur and result in loss of strength; in particular, magnesium may be lost or oxidized during welding due to its low boiling point.

Section 2.3.1 Porosity

Porosity occurs when gas is trapped in the molten weld metal and forms bubbles in the solidified weld. For aluminum, hydrogen acts as the culprit as it has high solubility in molten aluminum, about 20 times higher than solid aluminum[16], and can originate from a variety of sources including the filler and parent metal, contamination on the filler and parent metal, and

moisture in the shielding gas. By controlling weld bead shape, porosity can be reduced, as narrow and deep welds tend to trap individual pores during solidification. Appropriate welding parameters, such as a small current and short arc length, can also help to reduce the porosity level[17]; in addition, removing the oxide film on aluminum should be done before welding to reduce porosity.

Porosity is undesirable in welding because it can affect the strength of the welding area[18]; the hydrogen bubbles that become trapped in aluminum create tensile residual stresses near the surface of the material. These stresses expedite fatigue crack initiation following welding near the weld bead in both the longitudinal and transverse direction. One study from Poolperm et al. found that at a current of 130 A, welding speed of 210 mm/min, and a wire feed rate of 700 mm/min, the welded bead showed the highest porosity. These results suggested that at a lower current and welding speed, an increase in porosity is seen.

GTAW of AA 2024 with the occurrence of porosity results in negative impacts to mechanical properties including toughness, hardness, ductility, and stiffness, with residual stresses from uneven cooling causing distortion to the welded pieces.

Section 2.3.2 Partially melted zone (PMZ) cracking

Partially melted zone (PMZ) cracking, or liquation cracking, occurs in the region immediately outside the fusion zone where the base material is heated above the eutectic temperature and generally along the grain boundaries[19]. Pulsed current and arc oscillation during welding has been shown to reduce fusion zone and PMZ cracking, especially with low frequency oscillation GTAW[20]. Pulsed current lessens the extent of grain boundary melting, and arc oscillation decreases the distance between liquidus and eutectic phases through higher resultant velocity of the weld pool. Severity of PMZ cracking in welded AA 6061 with T6 temper can be attributed to severe grain boundary segregation of Si and Mg. Fusion zone composition

has a significant effect on PMZ cracking of AA 6061; aluminum liquids with greater amounts of silicon are considered to be more fluid, and the lower solidus temperature of 4xxx series aluminum alloys can promote liquid penetration into the PMZ.

Ductility of the fusion zone should also be considered, with chemical/metallurgical and mechanical factors playing an important role in susceptibility to PMZ cracking. If tensile strain is transferred from the PMZ area to the fusion zone partly or completely, PMZ cracking susceptibility decreases[19]. Fusion zone ductility can be increased using grain refinement and reducing PMZ cracking susceptibility; weld tensile residual stresses can be absorbed with a relatively finer grain size in the fusion zone.

Section 2.3.3 Post-weld treatments

Mechanical properties of weld joints depend on welding defects, composition, microstructure, and metallurgical states of the weld metal and neighboring base metal[3]. In heat-treatable alloys, the main causes of hardness reduction are loss of precipitates in the weld and overaging in the HAZ. Solution and aging heat treatments can be used to recover hardness in these areas. For AA 6061, the main issue associated with welding is the tendency of the weldment to overage and leading to deterioration in mechanical properties[11]. Post weld heat treatment (PWHT) is applied to relieve residual stresses and modify the microstructure, thus improving the mechanical and chemical properties of the fusion-welded joint.

When 4xxx series filler material is employed with 6061 base material, the weld zone does not respond to only post-weld aging as sufficient magnesium is not present for the precipitation of Mg_2Si, which is the main strengthening phase"[21] and requires solution heat treatment followed by artificial aging. Age hardening alone does not have a beneficial effect on tensile properties improvement; solutionizing followed by quenching allows closely packed atoms of the solute to uniformly distribute into the solution, with Guinier-Preston (GP) zones

forming after quenching which are connected with the solvent matrix. This process induces compressive stress fields near the weld joints and reduces tensile stresses. PWHT results in about 45% removal of postweld tensile residual stresses in GTAW AA 6061 alloys[22].

T6 heat treatment includes a solutionizing and age hardening process, with weldments heated at 530°C for one hour, quenched in water, and then artificially aged at 160°C for 18 hours[23]. A study from F. Fadaeifard et. al (2016) compared the mechanical properties of an AA 6061 welded plate with a thickness of 10 mm before and after T6 heat treatment. Before heat treatment, hardness values differed from 20 and 60 between the heat affected zone and the base material; however, after T6 heat treatment, a fairly uniform hardness profile is formed. The two hardness profiles can be seen below in Figure 2.3.3, with the top profile the as-welded sample and the bottom profile after PWHT.

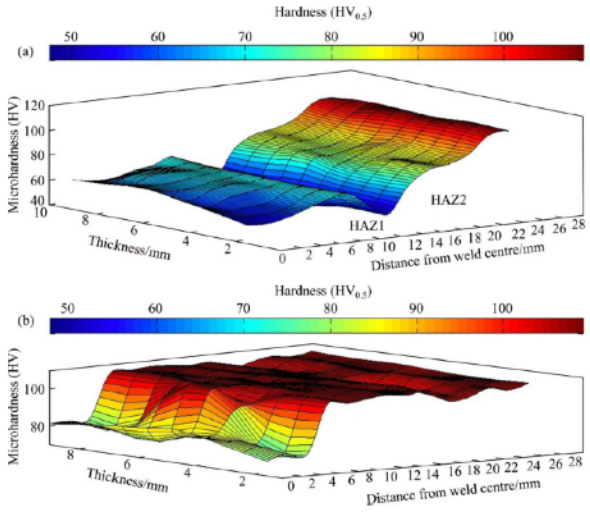

Figure 2.3.3 Hardness profiles for as-welded and PWHT AA 6061 samples[23]

Hardness values increase due to precipitation hardening and grain refinement during PWHT, with higher hardness values in particular near the HAZ.

PWHT changes the microstructure by allowing the Al_3Mg_2 (β-phase) intermetallic compound in the weld area to dissolve into the aluminum matrix during solutionizing at a

temperature above 450°C (the eutectic line). Therefore, the 560°C applied during T6 heat treatment allows the Al_3Mg_2 to completely dissolve into the matrix; however, α and β phases can form during age hardening at 160°C. The HAZ shows a uniform microstructure following PWHT, with yield strength increasing up to 54% and ultimate tensile strength increasing up to 50%[11]. However, as-welded samples show greater ductility in failure compared to PWHT samples, with shallow and big dimple-shape features along the fracture surface compared to the fine dimples shown in the fracture surface of as-welded samples. In addition, exposing the material to a temperature for longer than required can cause precipitates to grow too large and "more widely dispersed within the material"[21], causing the material to lose its strength and impose brittleness. Therefore, optimization of temperature and time are essential for the PWHT process.

The lowest hardness occurs in the solutionized HAZ for as-welded samples and in the weld zone for PWHT samples. Overall, PWHT samples show better uniformity and higher hardness from the homogenous microstructure and relieved residual stress.

Section 2.3.4 Problems associated with aluminum welding wires

Although largely defect free welds can be produced in difficult to weld 7xxx series alloys, severe problems still exist including poor properties in the fusion zone and lack of weldability — primarily due to commercially available aluminum filler wires not being specifically developed for high strength alloys such as 7075[24]. In addition, many applications require the weld bead to be removed in a post-weld machining operation, resulting in a lower joint efficiency from the reduced reinforcement. In unreinforced welds, failure generally occurs "within or at the edge of the fusion zone where, in alloys like 7150, the yield stress is typically ~50% that of the parent plate"[25]. Within the fusion zone, weld metal has low ductility and stiffness due to the large volume fraction of interconnected eutectic phases.

Popular, commercially available welding wires include AA 4043, AA 4943 and AA 5356. The strength and ductility of aluminum alloy joints is largely dependent on filler metals (FMs); the welded zone typically shows the lowest hardness values and resulting tensile strength in the as-welded condition. Low hardness values in the welded zone are typically associated with the lower tensile properties of the filler material selected[21]. The mechanical properties of these popular aluminum alloy fillers can be seen below, in Table 2.3.4.

Table 2.3.4 Mechanical Properties of Popular Aluminum Alloy Fillers

Aluminum Alloy	Density (g/cm^3)	Tensile Strength (MPa)
4043[26]	2.68	200
4943[27]	2.68	241
5356[28]	2.66	262

As shown in Table 1 in Section 1, typical base material alloys including AA 2024, 5083, 6061, and 7075 have tensile strengths in the heat treated condition ranging from 310 to 578 MPa. In the heat treated condition, AA 4943 achieves an ultimate tensile strength (UTS) of 338 MPa[29] — a slight increase from the 310 MPa value of 6061 T6 treated sample. This shows the critical nature of heat treating after welding to recover lost tensile strength.

Typically, fillers for welding heat treatable alloys have a lower melting temperature than the base alloy[7]. This allows the base metal alloy adjacent to the weld to solidify before the weld metal, minimizing the stresses on the base metal and reducing tendencies for intergranular cracking, or solidification cracking. However, solidification cracking remains a problem with commonly used filler material. Susceptibility to solidification cracking depends on several factors including the "solidification temperature range, the amount and distribution of liquid at the terminal stage of solidification, the primary solidification phase, the surface tension of the grain-boundary liquid, the grain structure, the ductility of the solidifying weld metal, and the tendency of weld-metal contraction and the degree of restraint"[12]. All of these factors are directly or indirectly affected by the weld filler material.

Unlike solidification cracking, the fracture surface in liquation cracking does not reveal a dendritic morphology and can occur in the grain interior. One study from Huang and Kou[30] found that if the solid fraction (f_s) of the weld filler metal exceeds the PMZ f_s during PMZ terminal solidification, "the solidifying and contracting weld metal can become stronger than the PMZ it pulls, and liquation cracking is likely to occur if tensile stresses/strains and liquidation are both significant in the PMZ." In particular, Huang and Kou fabricated full-penetration, circular-patch welds in 6061 aluminum with filler metals AA 5356 and AA 4043. This study found severe liquation cracking in the weld made with AA 5356 but not with the weld made with AA 4043. This can be attributed to the AA 5356 filler material having a greater f_s than the PMZ f_s during PMZ terminal solidification, while the AA 4043 filler had a f_s less than the PMZ f_s throughout PMZ solidification. A graph of solid fraction versus temperature can be seen below for these two weldments and the 6061 base metal in Figure 2.3.4.

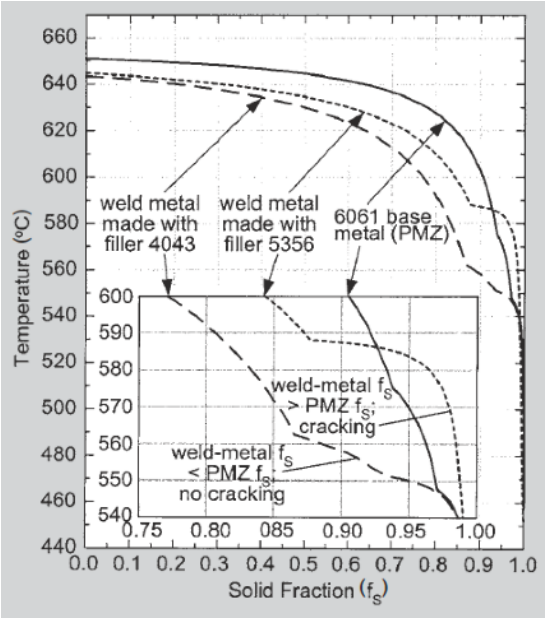

Figure 2.3.4 Solid fraction vs. temperature for AA 6061 weldments and base material[30]

Section 2.4 Effect of nanomaterial in welding processes

One of the most common methods for overcoming solidification cracking in aluminum alloys is through highly alloyed filler material to produce sufficient eutectic material and heal cracks through backfilling[9]. This includes the addition of grain refining elements such as titanium carbide (TiC) and titanium diboride (TiB_2) nanomaterial. As nanotech metallurgy develops, the use of rivets is being replaced by welding, bonding and extrusion, particularly for aluminum. Several studies have shown that adding nanomaterial in welding filler material improves the strength of welding electrodes[31,32] and enhanced well properties are achieved through the addition of nanoparticles to weld joints[33]. Nanoparticles that are uniformly dispersed ensure uniform cooling and microstructural formations in the weld metal; accumulation of particles must be considered to reduce negative effects on the joint[34,35]. TiC nanoparticles are typically selected for welding aluminum alloys as they are low density and offer good wear resistance and weldability[36]. Grain refinements in the weld from the addition of nanoparticles have shown additional improvement though the pinning effect offered by TiC nanoparticles in grain boundaries.

The reduction in grain size achieved through the addition of ceramic nanoparticles in the welded joint typically results in increased hardness of the material. The welded metal shows hardness below the base metal hardness due to the increased temperature above the recrystallization of the metal in the weld zone[37]. Improvement in hardness is achieved from grain refinement, increase of dislocation density, and formation of aluminum carbide[36]. The addition of ceramic nanoparticles in the filler metal allows the weld to increase grain refinement and improve hardness in the welded joint. Joint hardness is also increased through thermal strains caused by the difference in the thermal coefficient of expansion between aluminum and ceramic nanoparticles.

Ceramic nanoparticles added to the filler metal also produce increased ultimate tensile strength and yield strength[36]. This improvement is caused by the thermal mismatch between the ceramic nanoparticles and aluminum, which increases the dislocation density in the weld, as well as decreased grain size and obstruction of dislocation movement from the nanoparticles. In addition, fracture surfaces show ductile failure through dimples formed from addition of ceramic nanoparticles.

Research from M. Fattahi et al. fabricated nanocomposite AA 4043 welding wire with TiC nanoparticles through accumulated roll bonding (ARB), which achieved good dispersion of the TiC nanoparticles[38]. This filler material was used to weld 6061 aluminum alloy plates with dimensions of 150 mm x 100 mm x 10 mm as the base metal. These plates used a single V groove butt joint configuration with a 60° groove angle, and 160 A current and 1.5 mm s^{-1} for welding. Both 2.5% and 5% weight TiC filler material was prepared for comparison, and showed continuous reduction in grain size with increasing nanoparticle content. This improved grain refinement is due to Zener pinning, or the pinning force of nanoparticles on grain boundaries, and the heterogeneous nucleation on TiC nanoparticles. The Zener pinning force is expressed by the following equation:

$$F_z = f/Kr$$

where F_z is the particle pinning force, f is the particle volume fraction, K is the Zener coefficient and r is the particle radius. Nanoparticles tend to aggregate in the grain boundaries and slow grain boundary mobility.

The M. Fattahi et al. study found that hardness of the welds reinforced with TiC nanoparticles was significantly enhanced compared to unreinforced welds due to the presence of hard ceramic nanoparticles and grain refinement. Three different zones in the weld were analyzed: the welding zone, heat affected zone, and base metal. The weld zone showed increasing hardness with increasing nanoparticle content, while the heat affected zone and base

metal remained the same. In addition, both ultimate tensile and yield strengths increased and elongation decreased as the TiC nanoparticle content of the weld increased. Three possible strengthening mechanisms for nanoparticle-reinforced aluminum matrix composites (AMCs) include the thermal mismatch between the nanoparticles and matrix (strengthening by dislocation generation), grain size strengthening (Hall-Petch effect), and Orowan strengthening[38].

The Hall-Petch relationship was originally proposed in the 1950s for grain boundary strengthening in polycrystalline metals, and later expanded to plastic deformations and nanometer dimensions[39]. For polycrystalline metals and alloys, the Hall-Petch relationship is defined by the following equation:

$$\sigma_Y = \sigma_0 + Kd^{-1/2}$$

where σ_Y is the yield strength, σ_0 is the lattice friction stress, K is the Hall-Petch coefficient and d is the average grain size. This relationship has led to extensive research and development into refining grain size in order to increase the yield stress of polycrystalline metals and alloys as good agreement between yield stress and grain size has been found. The validity of the above equation has been proven down to a recrystallized grain size of about 3-4 μm[39] for aluminum, nickel, and copper. In particular, aluminum shows an experimental yield stress value that is significantly higher than the calculated value, possibly caused by powders that are slightly oxidized during processing. In addition, the Hall-Petch relationship is independent of the mode of synthesis, including by deformation followed by recrystallization, inert gas condensation, or by electrodeposition.

In the Orowan strengthening mechanism, the "movement of dislocations is effectively hindered by the presence of fine particles and thus increasing tensile strength of composite"[38]. The relative significance of this mechanism is found to increase with decreasing

size of nanoparticles until reaching a critical size of 1.74 nm for Mg/Al_2O_3 nano composites and 1.58 nm for Ti/Y_2O_3 nanocomposites[40].

Section 2.4.1 Production of aluminum nanocomposites

There are several approaches to manufacturing aluminum matrix nanocomposites, including solid state processing, liquid state methods, and semi-solid state processing[41]. Accumulative roll bonding (ARB) is a solid state method for fabricating aluminum nanocomposites, which can overcome problems associated with liquid state methods. This process involves "multiple cycles of surface treatment, stacking, rolling and cutting in which nanoparticles are well dispersed in the matrix with a strong interfacial bonding"[42]. ARB can lead to uniform dispersion of nanoparticles in the aluminum matrix through repetitions of this procedure; achieving a uniform dispersion of nanomaterial within the crystalline matrix is critical for enhancements to the mechanical properties of aluminum matrix nanocomposites.

Liquid state solidification processing is most promising for bulk manufacturing; however, "efficient feeding and dispersion of nano-reinforcements in crystalline matrix is still a great challenge." Problems include partial nano-reinforcement burning and loss during feeding and surface oxide formation. A typical setup for flux-assisted liquid state processing can be seen below in Figure 2.4.1.

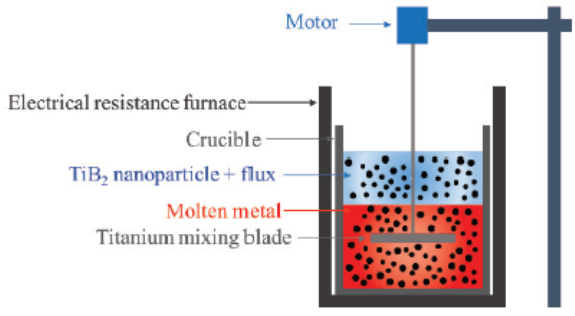

Figure 2.4.1 Flux-Assisted Liquid State Processing Setup[41]

Section 2.4.1.1 Casting of aluminum nanocomposite material

Casting following liquid state processing is the most economical route for making metal matrix composites (MMCs); however, it experience problems incorporating particles into the melt and can generate particle clusters during solidification processing[43]. In order to achieve good particle dispersion, the mechanisms preventing particles from being introduced into the melt and causing them to cluster must be understood. Barriers include surface oxide films, which can be reduced through the use of gas shields or fluxes, and wettability, which can be improved through vigorously stirring the melt; however, vigorous stirring can enable oxides, gases, and contaminants to be entrained into the melt and transfer of particles into the melt is not guaranteed. Poorly wetted particles have a tendency to agglomerate and vigorous stirring can promote more agglomeration through incorporation of gas bubbles, which attract particles due to the lower energy liquid-vapor interface. The reinforcement particles must be engulfed and wetted to form a strong interfacial bond and achieve effective load transfer from the matrix to the particle.

In a study done by A.R. Kennedy et. Al (1999), four different aluminum MMCs were casted: 5% volume TiB_2, 10% volume TiB_2, 5% volume TiC, and 10% volume TiC. Close to 100% of both TiC and TiB_2 nanoparticles were successfully incorporated into a casted aluminum charge, with TiC particles having slightly higher yield and resulting grain refinement. It was also found that as the volume fraction of particles increases, the composite grain size decreases; 10% volume additions grain size decreased only slightly, suggesting a smaller proportion of particles acting as grain nucleation sites after this point. Grain size results from this study are seen on the following page in Table 2.4.1.1, with samples taken 20 mm and 70 mm from the tip of a wedge-shaped mold.

Table 2.4.1.1 Grain sizes (in μm) before and after particle additions[43]

	99.7% Al	5 TiB_2	10 TiB_2	5 TiC	10 TiC
20 mm from tip	1500 ±250†	365 ±20	260 ±30	75 ±14	62 ±10
70 mm from tip	>4000†	560 ±80	475 ±65	112 ±20	92 ±18

†denotes highly elongated structures.

TiC particles showed an evenly spaced distribution with far fewer large clusters than TiB_2 in the castings. As TiB_2 particle fraction increased, the tendency for agglomeration also increased and showed less even distribution than TiC nanoparticles. TiC particles have improved wetting and an enhanced affinity for the aluminum melt, resulting in cleaner composites. In the Al-TiB_2 system, there are few sets of closely matching atomic planes than in the Al-TiC particle system, which forms an isomorphous melt. Few TiB_2 particles act as nucleation sites; however, they have an affinity for the solid phase and engulfment, resulting in increased ultimate tensile strength and stiffness with a high level of ductility for a cast material. Clusters of TiB_2 nanoparticles were observed in the metal grains, which suggests engulfment and agglomeration in the melt before solidification.

In a study completed by Javadi et al.[41], an aluminum 2% volume TiB_2 nanocomposite was compared to a pure aluminum ingot; hardness increase for the nanocomposite was found to be insignificant, most likely due to poor dispersion of the TiB_2 nanoparticles, as well as porosity and lux remnant in the nanocomposite. Improvement to the feeding efficiency may be needed to increase the incorporation of TiB_2 nanoparticles into the aluminum matrix.

Section 2.4.2 Stability of TiC in aluminum melts with silicon

AA 4943 has a relatively high silicon content compared to other aluminum alloys, at 5.0-6.0% by weight[27]. This provides it with high weldability as the silicon gives the alloy increased fluidity in the liquid state. One study from Ding Hai-min and Liu Xiang-fa[44] looked at the effect of silicon on stability of TiC in aluminum melts. As described previously, TiC has "high hardness and elastic modulus, low density and good wettability with molten aluminum" and are effective substrates for the nucleation of aluminum grains. This has made them the preferred option for nanophase material in aluminum metal matrix composites (MMCs).

However, TiC can easily react with elements in the aluminum melt and the refinement efficiency of TiC can be reduced. One such element is silicon, which has been shown to "remarkably influence" the stability of TiC[44]. The study from Ding et al. fabricated three Al-Ti-C master alloys — one with only aluminum and titanium carbide, one Al-Ti-C alloy with 7% mass silicon and another Al-Ti-C alloy with 13% mass silicon. X-ray diffraction (XRD) was used to determine the chemical composition of the samples and microstructures were analyzed using electron probe microanalysis (EPMA). In the pure Al-Ti-C alloy, a uniform distribution of TiC particles was observed. However, the samples with silicon exhibited disappeared TiC particles that transformed into a bright phase and a black block-like phase, with some of the bright phase being block-like and others needle-like. The bright phase contained mostly aluminum, titanium, and silicon elements, indicating "a kind of $TiAl_xSi_y$ ternary phase"[44], with the black, blocky phase containing mostly aluminum, carbon, and oxygen. The microstructures of the samples containing silicon can be seen below in Figure 2.4.2.

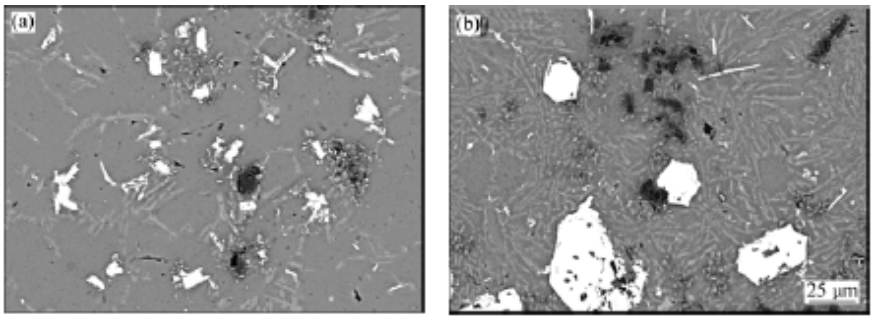

Figure 2.4.2 Microstructure of (a) Al-Ti-C alloy with 7% mass Si (b) Al-Ti-C alloy with 13% mass Si[44]

These reactions are also temperature dependent, with TiC particles reacting with Al and Si to form $TiAl_xSi_y$ and Al_4C_3 phases at 750 and 800°C, and blocky $TiAl_xSi_y$ phases disappearing at 900 and 1000°C to form new phases of Ti_3SiC_2. When the holding temperature is lower than 890°C, the reaction is as follows:

$$TiC + Al\ (l) \rightarrow Al_4C_3 + Ti\ (l)$$

When the holding temperature is higher than 890°C, the reaction is as follows:

$$TiC + Si\ (l) \rightarrow Al_4C_3 + Ti_3SiC_2$$

The stability of TiC in the Al melt is directly related to the number of carbon vacancies in the crystal structure of TiC, as these particles are never found experimentally to be fully stoichiometric[44]. Formation energies of Al and Si substituting C vacancies in TiC are +0.98 eV and -3.89 eV, respectively, allowing Si to more easily penetrate into TiC than Al — resulting ins Si-containing TiC in the Al-Si melt.

Section 2.4.3 Microstructure study

Grain size has a tremendous influence on the mechanical properties of aluminum alloys and determination of grain size, shape, and distribution is very important[45]. There are many methods to reveal the grain structure of aluminum and its alloys, including mechanical polishing, electrolytic polishing, chemical etching, and electro-etching[46]. Anodizing techniques

and chemical etchants, such as Weck's reagent, are commonly used. Weck's reagent, in particular, is very sensitive to micro-segregations of titanium, silicon, and magnesium in aluminum alloys[47]. This color etchant was developed in the 1980s by Weck and Leistner[48] and contains 4 g of $KMnO_4$, 1 g of NaOH, and 100 mL of distilled water. Micro-segregations formed during solidification of the aluminum phase are revealed by color differences between central and surrounding regions using this etchant.

One study from Li Gao et al. (2015) used four different materials to compare the effectiveness of Weck's reagent: A356 with titanium, titanium-free A356, aluminum with 7% weight silicon, and aluminum with 5% weight magnesium. Since A356 contains both silicon and magnesium, the Al-Si and Al-Mg binary alloys were created to demonstrate the effects of Weck's reagent on aluminum with silicon and magnesium, separately. Specimens were immersed in Weck's reagent for approximately 12 s at room temperature, and the microstructure was observed by optical microscopy (OM). One specimen was etched five times, for 4 s, 8 s, 12 s, 20 s, and 28s to study the influence of etching time. Before each etching, the surface was polished to remove the previous etching layer.

Micro-segregations of silicon and magnesium were confirmed in the titanium-free A356 alloy using electron probe micro-analysis (EPMA) mapping. Both materials dilute in the center region of the aluminum dendrite and concentrate gradually towards the eutectic region. However, color contrast is much lower than the Ti-contained alloy due to the huge difference in the diffusion speed of solutes in the aluminum phase; the diffusion coefficient of titanium in aluminum is much lower than silicon and magnesium. In this way, Weck's reagent helps to visualize grain growth and can be used as a modified quantitative metallography.

The Weck's reagent etching process can be described by the following chemical reaction[49]:

$$Al + MnO_4^- + 2H_2O \rightarrow Al(OH)_4^- + MnO_2$$

The MnO_2 film is formed on the surface of the specimen after etching. Color changes from location to location due to different concentrations of the aluminum solute across the specimen, resulting in differing thicknesses of the MnO_2 film. Different elements in the alloy, such as silicon and magnesium, can also affect the reaction and result in color differences. Images of the Al-7Si binary alloy before and after etching with Weck's reagent can be seen below in Figure 2.4.3:

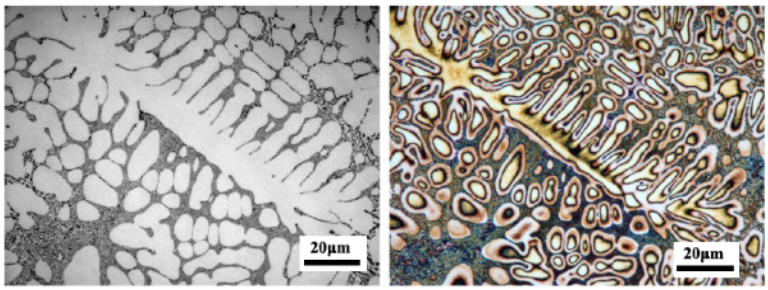

Figure 2.4.3 Al-7Si binary alloy (a) before and (b) after etching with Weck's reagent[47]

The etching result using Weck's reagent is very sensitive to etching time; 12 s delivered the best contrast in Li Gao et al. study. Good re-producibility was achieved with invariable color across several samples etched for 12 s. In addition, it was confirmed that Weck's can be used to reveal grain boundaries; electron backscatter diffraction analysis (EBSD) was used to confirm the existence of high angle grain boundaries (HAGBs) within the aluminum phase, which form during recrystallization following solutionizing. These boundaries corresponded with lines in the OM images of the etched sample.

ASTM provides recommendations for methods to microetch metals and alloys[50]; for 4xxx series aluminum, etchants are available to determine the general structure. However, there are no recommendations for etchants to observe grain structure under polarized light and phase identifications. 2xxx, 5xxx, 6xxx, and 7xxx series alloys all have recommendations for both general structure and phase identifications; 6xxx and 7xxx series also have recommendations

for grain structure under polarized light. The recommended etchants for aluminum alloys can be seen below in Table 2.4.3, with corresponding etchants shown in Appendix 1.

Table 2.4.3 ASTM recommended etching methods for aluminum alloys[50]

Metal	Etchants	Uses
Aluminum Base:		
Pure Al	1a, 2, 3 *4*, 5 1b	general structure grain structure under polarized light grain boundaries and slip lines
1000 series	1a, 3, 2 *4*, 5 6, 7	general structure grain structure under polarized light phase identifications
2000 series	3, 2, 1a 8a, 6, 7	general structure phase identifications
3000 series	3, 1a *4*, 5 8a, 6, 7	general structure grain structure under polarized light phase identifications
4000 series	3, 1a	general structure
5000 series	3, 1a, 2, 6, 8a *4*, 5	general structure grain structure under polarized light
6000 series	3, 1a, 2, 6, 8a, 222 *4*, 5 1a, 2, 7, 6, 8a	general structure grain structure under polarized light phase identifications
7000 series	3, 1a, 2 *4*, 5 3b, 6	general structure grain structure under polarized light phase identifications

All etching is intended to be carried on freshly polished samples, with gentle agitation during immersion for a more uniform etch.

Grain contrast can vary greatly with standard chemical etching and anodizing techniques between different aluminum alloys and heat treatment conditions; multiple etching periods with more than one solution can be used in order to fully develop the structure of the specimen. In order to improve grain structure determination for 2xxx and 5xxx series aluminum alloys, one study from M. Mohammadtaheri used a multi-step process to develop the microstructure. A pre-etchant solution of 1 gram NaCl in 50 mL of H_3PO_4 was first used for three minutes at 70°C, followed by etching in Weck's reagent. The pre-etchant affects precipitates and grain boundaries, while the Weck's reagent produces a positive effect on the grain contrast.

This study shows how utilizing multiple etching periods with different solutions can lead to more accurate microstructure results.

A combination of electrolytic etching and Barker's reagent is another common method for microstructure determination of aluminum; Barker's reagent is composed of 4-5 mL HBF_4 and 200 mL distilled water[46]. This method uses a 20V direct current with the aluminum sample as the anode and aluminum scrap material as the cathode. A current of 0.1-0.4 A/cm^2 is maintained during the electrolytic etching process for commercially pure aluminum.

III.Experimental Procedure

Section 3.1 Fabrication of aluminum nanocomposite wire

In order to run experiments to compare the use of 4943 nanocomposite filler material with standard 4943 filler material in aluminum welds, nanocomposite filler wires were fabricated by casting a 4943 aluminum alloy with titanium diboride (TiB_2) nanoparticles. A nanocomposite aluminum master was used that was approximately 3% by volume TiB_2, along with additional aluminum to achieve 1% by volume TiB_2 in the filler casting. In a second round of casting, the nanocomposite filler achieved 1.25% by volume TiB_2. An aluminum-magnesium master of about 25% by weight magnesium and pure silicon was also implemented in both castings to achieve 4943 aluminum alloy composition, which contains between 5.0-6.0% by weight silicon and 0.1-0.5% by weight magnesium[27]. The recipe for the 4943 1%v TiB_2 and 1.25%v TiB_2 filler material can be seen below in Table 3.1.

Table 3.1 4943 Nanocomposite Filler Composition

	4943 1% volume TiB_2		4943 1.25% volume TiB_2	
Material	**Volume**	**Mass**	**Volume**	**Mass**
Aluminum	55.56	150	103.7	280
TiB_2	0.61	2.74	1.39	6.3
Magnesium	0.47	0.8	0.88	1.5
Silicon	3.78	8.78	7.06	16.38
Total	**60.42**	**162.32**	**113.03**	**304.18**

During the alloying process, the mold to cast the filler material was first clamped and heated using a furnace (up to 400°C) to prevent solidification of the aluminum MMC before completely filling the mold. A crucible was placed into another furnace and allowed to heat up; aluminum was then added and heated up to 750°C, or just above its melting temperature as the addition of more material caused the temperature to drop. Argon gas was fed into the bottom of the furnace to prevent oxidation of the aluminum; as the aluminum melted, oxidation on the surface was removed revealing a reflective surface due to the argon protection. Silicon

was then added, which dissolved into the aluminum, followed by the aluminum-TiB_2 master. Magnesium was then added with SF_6 gas turned on to serve as a protective medium to prevent oxidation and evaporation of the magnesium. A temperature below 800°C was maintained to limit the amount of magnesium that could oxidize and/or evaporate. The furnace used to complete the alloying process can be seen below in Figure 3.1, with a protective thermal insulation layer resting on top.

Figure 3.1.a Furnace for Alloying 4943 Nanocomposite Filler Material

Following melting of the materials in the crucible, the alloy melt was stirred with a mixer for approximately one minute and then poured into a steel mold to create a prismatic shape of 6 mm thickness, facilitating fabrication of nanocomposite welding wire. After the casting was completed and allowed to cool, samples were taken from the 4943 1% volume TiB_2 and 1.25% volume TiB_2 alloys at the top and bottom. This was done to ensure homogenous material properties throughout the casting, including TiB_2 nanoparticle dispersion. Results from this characterization are discussed below in Section 4.1.

The resulting prismatic nanocomposite filler material was then hot rolled to achieve a thickness of approximately 3 mm, or the thickness desired for the welding wire. Before hot

rolling, the 1.25% volume TiB_2 material was heated for 1.5 hours at 510°C and quenched in water to solutionize the secondary phase and increase ductility for hot rolling. The material was then hot rolled with 20% reductions in thickness until achieving a thickness of 3 mm. Following hot rolling, the water jet cutter was used to obtain strips of welding wire with widths of about 3 mm and dimensions appropriate for feeding during the arc welding process. The casted filler material after hot rolling and resultant welding wire strips can be seen below in Figure 3.1.b.

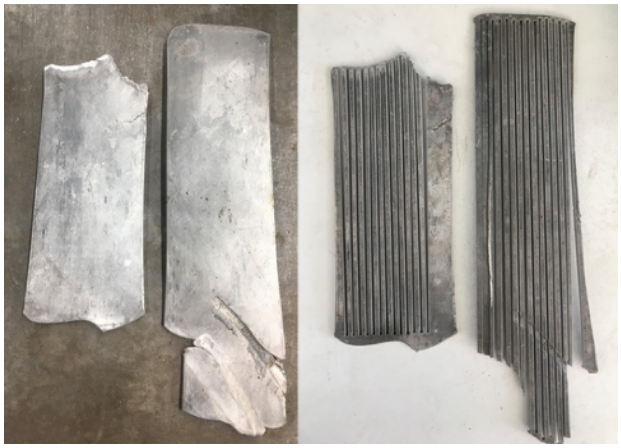

Figure 3.1.b 4943 1.25%v TiB_2 Filler (a) after hot rolling and (b) after water jet cutting

After the appropriate dimensions for welding wire were achieved from the casted filler material, the resultant strips were ground with a sanding tool and rubbed with Scotch-Brite scouring pads to remove the outside layer of dirt and surface imperfections. The smoothed strips were then brushed with acetone to remove any remaining dirt on the surface.

To fabricate long lengths of the 4943 nanocomposite welding wire, the 3 mm thick wire strips were tacked together using the TIG welder set at a very low amperage of about 30 A. Strip lengths were placed overlapping eachother and the TIG arc welder was activated for approximately one second to fuse strips together into longer lengths. After obtaining longer welding wire lengths, the wire was ready for welding aluminum plates.

Section 3.2 Welding aluminum plates & parameters

Initially, aluminum alloy plates of 3 mm with dimensions of 38 mm by 76 mm were cut using the water jet cutter. However, it was found that these dimensions were too small in order to get accurate characterization samples, due to the heat from welding affecting the entirety of the plate. It was then decided to use aluminum alloy plates of 3 mm thickness, cut into desired dimensions of 76 mm by 152 mm using the water jet cutter, or about twice the size of the plates that were previously cut. After the appropriate length and width were achieved, the long edge (152 mm) was sanded and polished to create an approximately 30° along the welding edge. This angled edge created a single V groove butt joint when two plates were welded together along the angled edges; this joint is easily designed and uses a minimum amount of material[3].

Following sanding and polishing to create angled edges, the edges were then rubbed with Scotch-Brite scouring pads to further smooth out the welding surface, and then finished with acetone to remove any remaining debris. This ensured a smooth, clean surface along the the single-V butt joint. Plates were then tacked together on both ends of the weld length to hold the plates in place during welding. This was accomplished using the TIG welder at 120 A and leaving a small root gap between the plates. In addition, alternating current (AC) polarity at a frequency of 180 to 200 Hz was selected, with a high frequency start and pedal pressure output. The arc was used to heat up one plate corner to a molten state, filler material was melted into the groove, the other plate corner was heated to a molten state, and the tack was formed by moving the arc between the two corners.

Following tacking, a welding robot was used to complete the linear weld length. This robot used an oscillating tip in order to increase welding solidification rate, as oscillation increases forward movement, and to account for potential alignment issues. Forward movement is also used to automatically heat the V groove evenly and allow for the manual addition of filler

material during operation. Amperage of the TIG welder was kept at 150 A during this process. Following completion of the linear weld, the plates were immediately removed from the copper backing plate and allowed to cool to minimize effects of the heat from welding on the weld joint's mechanical properties.

Section 3.3 Preparing welds for characterization

After completion of the welds, they were prepared for characterization by cutting samples of about 12 mm width from areas of the weld with excellent penetration and away from heated tacking zones on either end of the weld. An example of cut lines can be seen below in Figure 3.3, where AA 2024 & 2024 weld with standard 4943 filler material was cut. The water jet cutter was used to quickly cut these samples.

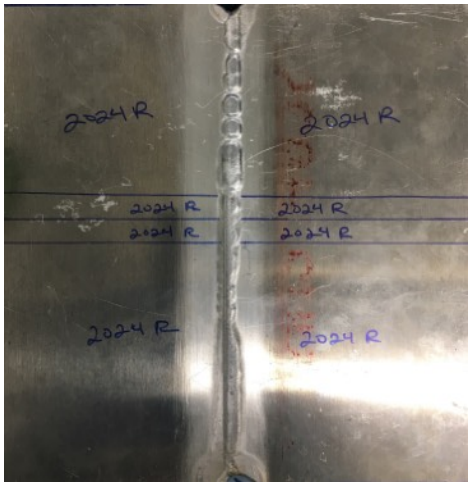

Figure 3.3 Cut Lines Along 2024 & 2024 Weld Length

For welds that were cut with the wire EDM to prepare tensile bars (discussed below in Section 3.6), leftover areas not used for tensile testing were used to characterize the welds. The samples cut by water jet and EDM were then polished to allow for characterization with the optical microscope, microhardness tester, and chemical etchants. Polishing paper from 60 grit to

1200 grit were used to gradually smooth the surface; the surface was finished using silica suspension to achieve a reflective surface.

For the AA 6061 & 6061 welds, a T6 heat treatment was achieved by first solutionizing, quenching, and artificially aging some of the tensile bars and cut samples. These pieces were placed in the furnace at 530°C for about 1.5 hours, and then quenched in water. The furnace was then allowed to cool to 160°C, and the tensile bars and samples were placed back inside and allowed to bake at 160°C for 18 hours.

Section 3.4 Microhardness procedure

Microhardness testing was completed on all samples with the microhardness tester set at 1.33 kN load and 10 seconds of dwell time. Readings were taken from the fusion zone on each side of the weld at 1.3 mm spacing with two readings taken for each linear spacing. Approximately 22.9 mm of readings were taken on each side of the weld zone from the fusion zone outward to determine values for the complete heat affected zone. This resulted in about 18 linear hardness values on each side (after 36 readings were averaged), and 5 readings taken from the weld zone, for about 41 readings in total. This provided a clear understanding of the trend in hardness values across the weld pool, heat affected zone, and base material.

Section 3.5 Etching procedure

Weck's reagent was used to determine the microstructure of samples containing 2xxx and 7xxx series aluminum alloys. In general, an initial etching cycle of 15 seconds with the sample immersed in the Weck's reagent was implemented and checked with OM. After determining whether this initial cycle was enough to obtain color contrast in the grain boundaries, additional cycles of 5 seconds were implemented until achieving the desired contrast.

Electrochemical etching was also used with Barker's reagent to determine the microstructure of samples with AA 5083. This process included applying an electrical current through the welded sample, with the sample serving as the anode and another piece of aluminum as the cathode. A voltage of approximately 0.1 V was applied, with current kept low as possible during etching. Etching cycles of approximately 25 seconds were used, with additional cycles of 25 seconds applied as necessary.

Section 3.6 Tensile testing

Tensile testing is an important component of the characterization process as it provides critical information on the strength and ductility of materials under uniaxial tensile stresses, which is useful to compare different materials and designs[51]. To cut tensile bars from prepared welds, AgieCharmilles CUT 200 Sp was used with prepared g-code to cut 7 tensile bars. After confirming the geometry of the cut as well as operation parameters including material, thickness of the material, wire material/diameter, and number of passes (one in this case), the machine was zero-d on the side at the center of the weld bead. The wire cutter was then moved to the zero point of the g-code, located 89 mm from the centerline of the weld bead on the corner of the aluminum plate. The geometry and operation was then executed with the speed and tension in the wire being observed to ensure optimization of parametersi. The speed of the EDM cutting noticeably slowed down in the weld zone, as the filler material was less conductive than the base material due to secondary phase and nanophase around the aluminum matrix.

Tensile bars were cut according to ASTM standard E8[51], which provides dimensions for plate-type and sheet-type samples. These dimensions can be seen below in along with the resulting tensile bars in Figure 3.6.a.

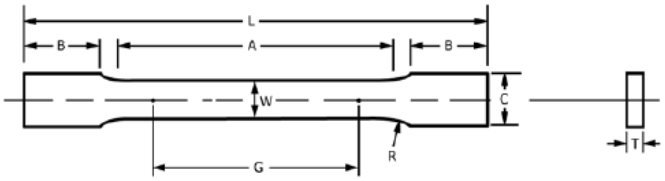

	Dimensions, Plate-Type, 40 mm wide	Dimensions, Sheet-Type, 12.5 mm wide
G — Gauge length	200.0 ± 0.2	50.0 ± 0.1
W — Width	40.0 ± 2.0	12.5 ± 0.2
R — Radius of fillet (min)	25	12.5
L — Overall length (min)	450	200
A — Length of reduced parallel section (min)	225	57
B — Length of grip section (min)	75	50
C — Width of grip section (approximate)	50	20

Figure 3.6.a ASTM tensile bar dimensions for plate-type samples[51]

Sheet-type samples range in nominal thickness from 0.13 to 19 nm. Given the aluminum plates welded had a thickness of 3.2 mm, dimensions for sheet-type samples were used.

Before testing, the samples were face milled to remove the protruded weld bead and form flat samples. In order to ensure the ultimate tensile strength of the material could be reached with the tester, an ultimate tensile strength of 310 MPa was assumed for the 6061 weld with T6 heat treatment[52]. Using this value, as well as the 12.7 mm width along the center of the tensile bar, a thickness (T) of approximately 2.5 mm was calculated in order to stay within the limit of the tensile tester, which had an ultimate tensile testing capacity of up to 10 kN. The areas remaining in between the cut tensile bars were then used to characterize the welds, described below in section 4.2. Resulting tensile bars can be seen below in Figure 3.6.b.

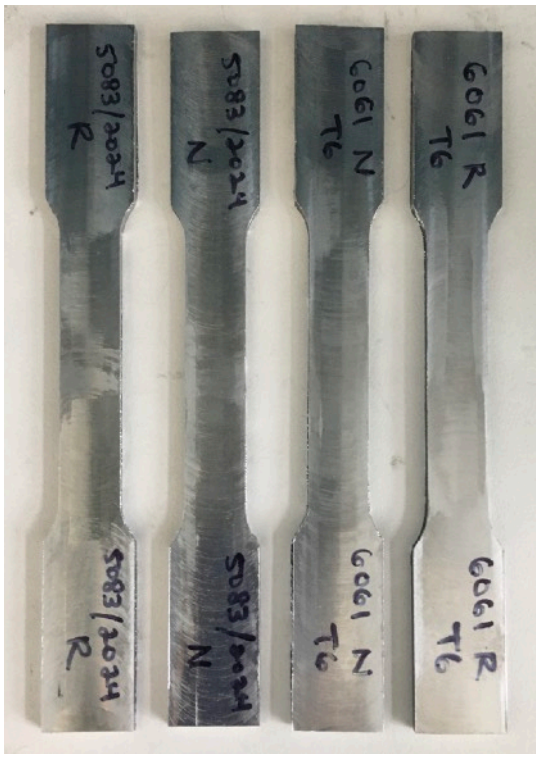

Figure 3.6.b Cut tensile bars after facing

IV. Experimental Results

Section 4.1 Characterization of nanocomposite 4943 filler material

After casting of the nanocomposite 4943 filler material was completed, samples were cut from the top and bottom of the casted material, polished and characterized with an optical microscope to ensure homogenous properties throughout the material. Originally a 4943 1% volume titanium carbide (TiC) filler was cast, as TiC nanoparticles showed superior dispersion and grain refinement throughout other aluminum alloys. However, after polishing a sample of the newly casted 4943 TiC nanocomposite, clusters of material and dark, block-like areas where a reaction had taken place was clearly visible with optical microscope. One such area can be seen below in Figure 4.1.a.

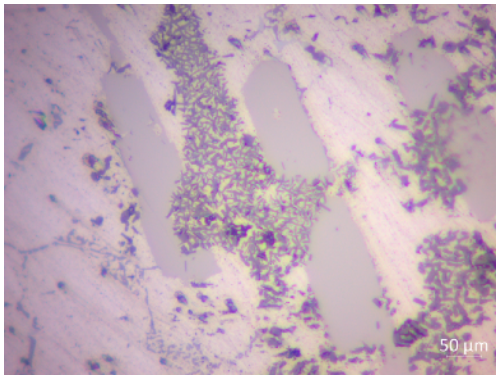

Figure 4.1.a Casted 4943 1% volume TiC reactions

In order to get a better understanding of the composition of these areas where a reaction had clearly occurred, scanning electron microscopy (SEM) was used with X-ray diffraction (XRD). The images obtained from this process can be seen on the next page in Figure 4.1.b.

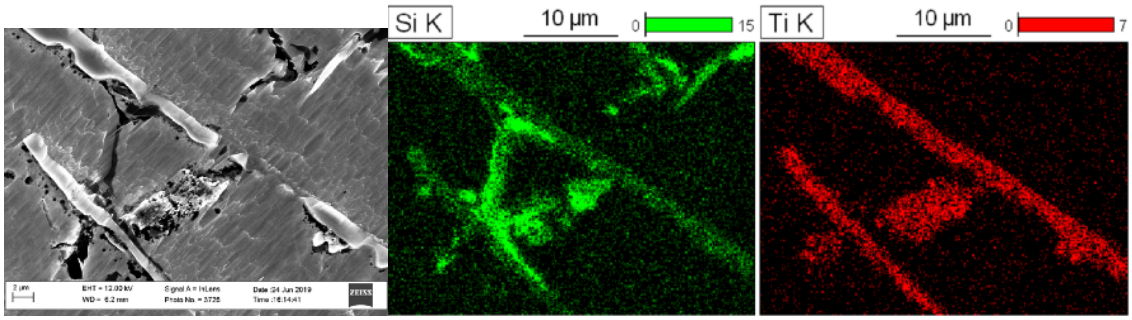

Figure 4.1.b SEM Images of 4943 1%v TiC

As discussed in section 2.4.2, TiC reacted with silicon in the 4943 aluminum alloy melt to create clusters of titanium and silicon. This ternary phase can be detrimental to the mechanical properties of the welded joint and can cause stress concentrations resulting in cracking and fracture. Therefore, TiB_2 nanoparticles were used in the casted AA 4943, as this material remained intact in the AA 4943 melt and did not show the same reaction with silicon as was seen with TiC.

Following casting of AA 4943 with 1% volume TiB_2, samples were characterized from the top and bottom of the casted material, as was done with the AA 4943 TiC nanocomposite. Large clusters of secondary phase containing TiB_2 nanoparticles were observed in both the top and bottom of the cast. As discussed previously in section 2.4.1, TiB_2 nanoparticles show less even distribution than TiC nanoparticles in the aluminum melt and agglomerate before solidification. However, the potential for increases to tensile strength and other mechanical enhancement remains due to TiB_2 particles' affinity for the solid phase and engulfment in the aluminum matrix[44]. The optical microscope results of the AA 4943 1% volume TiB_2 casted material can be seen on the next page in Figure 4.1.c.

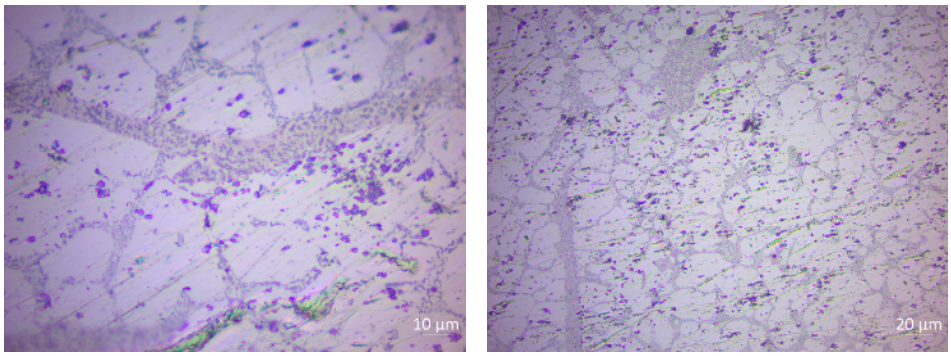

Figure 4.1.c OM images from (a) bottom and (b) top of the AA 4943 1% volume TiB_2 cast

Despite clustering, a relatively even amount of TiB_2 nanomaterial was observed in both the top and bottom of the cast. Therefore, uniform distribution of TiB_2 in the casted material was assumed and the cast was used to weld small trial plates (38 mm x 76 mm x 3 mm) as well as the larger plates that would be used for characterization (76 mm x 152 mm x 3 mm).

After welding the AA 2024 & 5083 and AA 7075 & 7075 welds with AA 4943 1% volume TiB_2 filler and the larger base material plates, more filler was cast to fabricate the additional three nanocomposite welds from the larger plates — AA 6061 & 6061, AA 5083 & 5083, and AA 2024 & 2024. The recipe was modified with additional TiB_2 nanoparticles of 1.25% volume in this batch. The casted filler showed dendritic secondary phase of silicon and magnesium, with occasional clusters of TiB_2 nanoparticles. OM images from the 1.25% volume TiB_2 cast can be seen below in Figure 4.1.d:

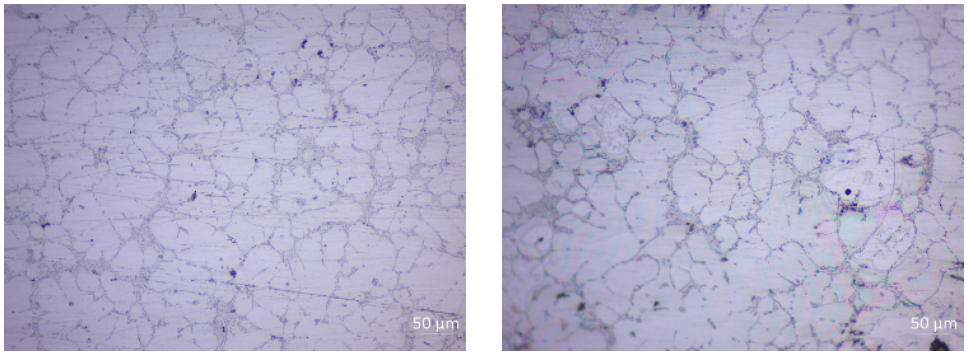

Figure 4.1.d OM images from (a) bottom and (b) top of the AA 4943 1.25% volume TiB_2 cast

These images show similarity in distribution of the secondary phase with clusters of TiB_2 nanoparticles observed in both samples. Thus it was assumed that the casting achieved homogenous properties throughout the mold and avoided nanophase material settling at the bottom or other irregularities. This material was then ready to be used as welding filler wire.

Section 4.2 Characterization of welded material

Initially, small plates of dimensions 38 mm x 76 mm x 3 mm were welded together with reference AA 4943 filler and nanocomposite AA 4943. Due to the massive heat input from welding, these samples showed distorted microhardness profiles from solutionization of the base material. This confirmed the need for a larger plate size in order to get accurate microhardness readings and other mechanical properties. Samples from this process can be seen below in Figure 4.2.a.

Figure 4.2.a Initial welding samples with small plates

The larger plates of dimensions 76 mm x 152 mm x 3 mm were then welded together with reference AA 4943 filler material and nanocomposite AA 4943 filler material. Mixed results were seen with filler penetration, as shown on the next page in Figure 4.2.b.

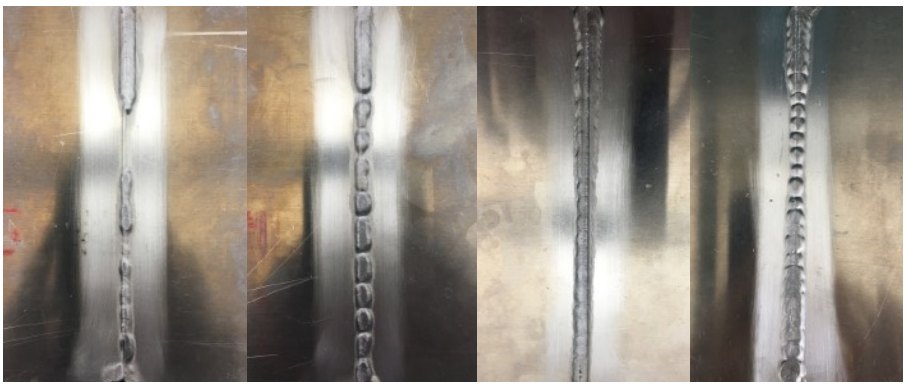

Figure 4.2.b Weld filler penetration for (a) AA 7075 nanocomposite, (b) AA 7075 reference, (c) AA 6061 nanocomposite, (d) AA 6061 reference

In some cases, such as with the AA 7075 & 7075 noncomposite filler weld, penetration was affected by not leaving a sufficient enough root gap between the plates after tacking. As shown previously in Figure 2.1.2, a specified root gap is put in place which allows filler material to penetrate and fuse with the back side of the plates. However, tacking on either end of the plates before the linear weld caused the plates to be forced together, and in some cases removed the root gap. A distance of approximately 5 mm was needed before tacking to leave sufficient root gap. In addition, increasing the current in the GTA welder helped improve penetration. In general, a current of 150 A was used for welding of the plates; however, for plates where root gap was insufficient, the current was increased to 155 A, which noticeably improved penetration of the filler material.

Following welding of the aluminum plates with both the nanocomposite AA 4943 filler material as well as the reference AA 4943 filler for comparison, characterization of the welded joints was completed to determine mechanical properties. These characterization processes included microhardness testing, optical microscope imaging with microstructure determination, and tensile testing.

Section 4.2.1 Microhardness

For the 7075 & 7075 weld, microhardness across the weld profile for both heat affected zones and weld zone showed similar values with the 4943 1% volume TiB_2 filler and the 4943 reference filler. This profile can be seen below in Figure 4.2.1.a.

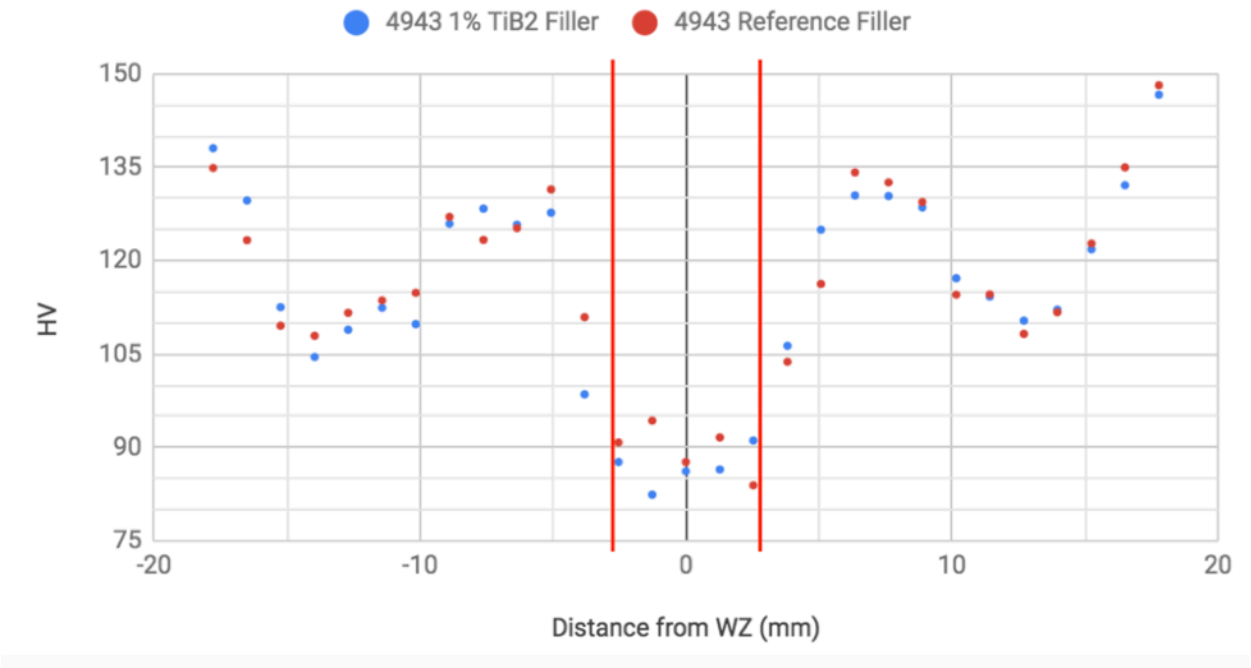

Figure 4.2.1.a AA 7075 & 7075 Weld Hardness Values

The heat generated during the GTA welding process caused a dip in the hardness values around the weld zone, before recovering on either side to the typical hardness value of AA 7075. A peak in hardness, up to 134 VHN, is seen close to the fusion zone before dropping back down due to the effects of heat. This peak is possibly due a "large faction of alloying elements in solid solution at the end of the weld thermal cycle, thereby giving conditions for extensive age hardening"[7]. Precipitate dissolution occurs in this area, which enriches the solid solution of the aluminum matrix with alloying elements and increases the hardness.

Hardness in the area of the weld zone for the AA 7075 & 7075 weld averages 86.8 VHN for the weld with AA 4943 1% volume TiB_2 filler material and 89.7 for the weld with 4943

reference filler material. In general, hardness values for the weld with 4943 reference filler trend slightly higher in the weld zone and also in the HAZ, with the nanocomposite filler weld averaging 117.5 and the reference filler weld averaging 118.2. Thus, the effectiveness of utilizing nanocomposite 4943 filler material for 7075 welds is questionable given the slight reduction in hardness values from welds with standard 4943 filler.

The AA 2024 & AA 2024 welds showed a similar trend, with hardness values for the weld with reference AA 4943 filler material trending slightly higher than the welds with AA 4943 1.25% volume TiB_2 filler material. This hardness profile can be seen below in Figure 4.2.1.b.

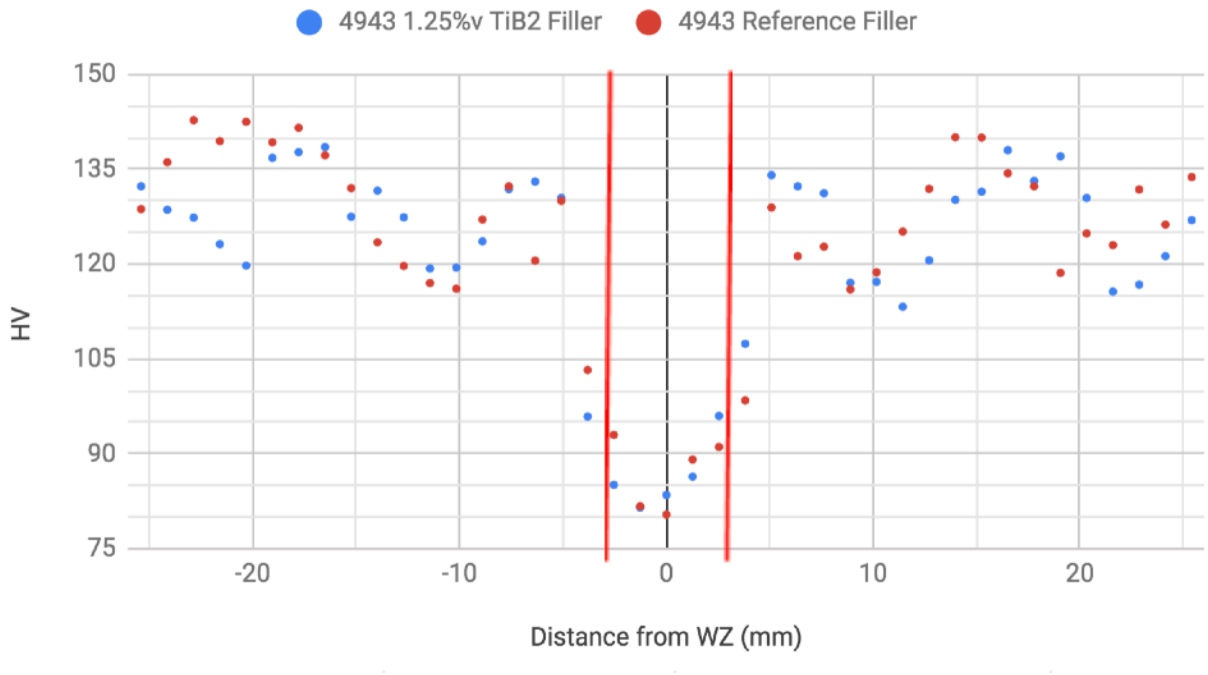

Figure 4.2.1.b AA 2024 & 2024 Weld Hardness Values

Within the weld zone, the nanocomposite filler weld averaged 86.5, while the reference filler weld averaged 87.1. Within the HAZs, the nanocomposite filler weld averaged 125.9, while the reference filler weld averaged 127.3.

For the AA 6061 & 6061 weld, minor increases were seen in the weld zone from the sample with 4943 reference filler to the sample with 4943 1.25% volume TiB_2 filler material. For

the 4943 reference filler sample before heat treatment, values averaged about 71 Vickers hardness, while the 4943 1.25% volume TiB2 filler sample averaged about 75.2 Vickers hardness. The increase in weld zone hardness was more drastic for the T6 heated samples, with the 4943 reference filler sample averaging 108.3 Vickers hardness in the weld zone, and the 4943 1.25% volume TiB_2 filler sample averaging 127 Vickers hardness in the weld zone. This profile can be seen below in Figure 4.2.1.c.

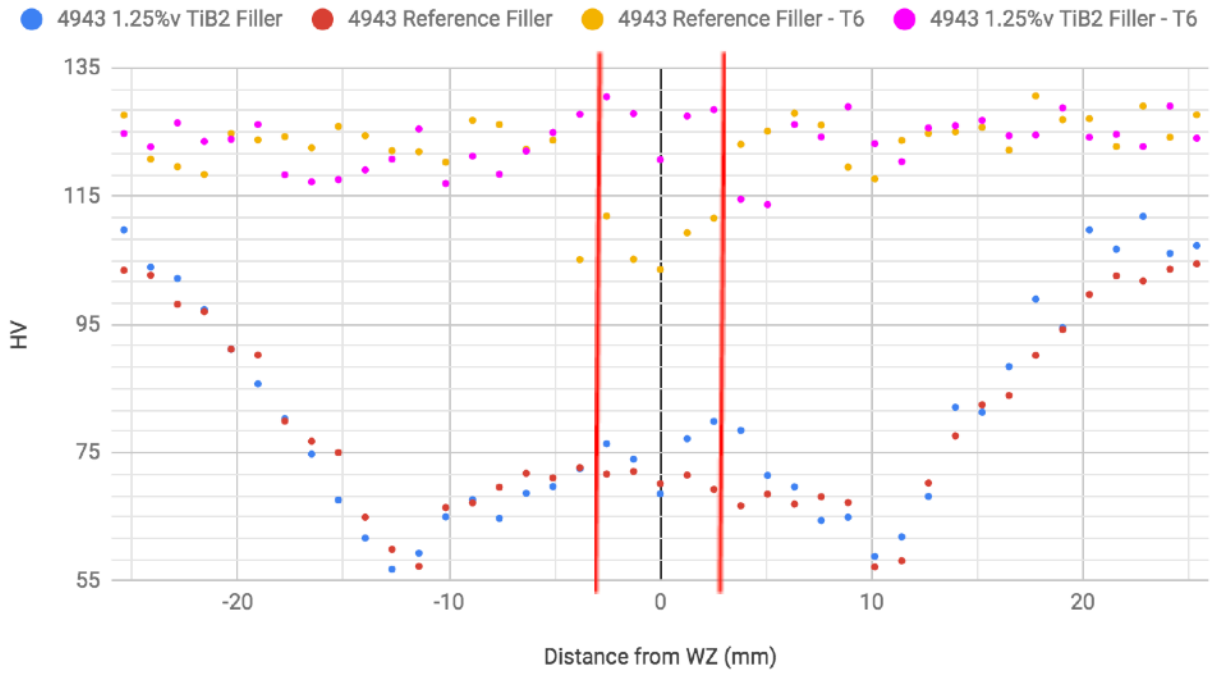

Figure 4.2.1.c AA 6061 & 6061 Weld Hardness Values

Substantial improvements to the hardness values for the T6 heat treated samples occurs due to precipitation of metastable phases during aging[7]. Superior tensile properties can be observed from these samples due to a uniform distribution of precipitates within the aluminum matrix and a higher amount of precipitates in the weld region. The decreasing trend in hardness values on the right of the weld zone for the AA 6061 & 6061 T6 with 4943 1.25% volume TiB_2 can be explained through solutionizing.

For the dissimilar weld using AA 2024 & 5083, it was found that using additional nanomaterial in the filler, or 1.25% volume TiB_2 over 1% volume TiB_2, led to improvements in the microhardness values. The sample with AA 4943 1% volume TiB_2 filler averaged 84.7 VHN in the weld zone, while the AA 4943 1.25% volume TiB_2 filler sample averaged 98.7 VHN in the weld zone. Between the two reference welds, hardness values averaged 97.5 VHN in the weld zone, fairly close to the weld zone average for the 1.25% volume TiB_2 filler sample. The microhardness profile for these samples can be seen below in Figure 4.2.1.d.

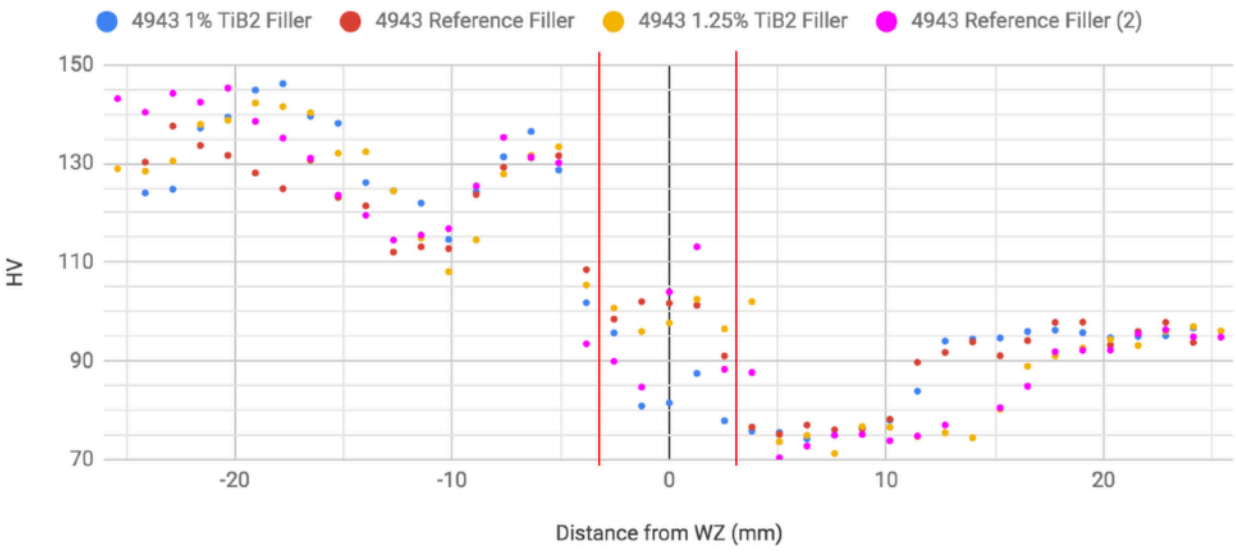

Figure 4.2.1.d AA 2024 & 5083 Weld Hardness Values

After compiling microhardness results for all of the welds with both reference and nanocomposite 4943 filler material, it was decided that due to the slight increases in microhardness in the weld zone for the AA 6061 & 6061 and AA 2024 & 5083 using nanocomposite 4943 filler material, these samples were of most interest for tensile testing. The microhardness results are then confirmed through the ultimate tensile strength of the samples.

Section 4.2.2 Optical observations

Optical microscope images were also taken for samples after polishing to confirm welding results, in particular with respect to porosity, intermetallic phases, and fusion zone characteristics. For both the AA 6061 & 6061 and AA 5083 & 5083 welds with AA 4943 1% volume TiB_2 filler, large clusters of secondary phase containing TiB_2 nanoparticles were observed in the weld zone, consistent to what was seen in the casted material in section 4.1. Long, "finger-like" cluster zones of secondary phase and TiB2 nanoparticles are shown in both the casted sample of AA 4943 1% TiB2 in Figure 4.1.c, as well as in the optical images of the weld zone for the welds seen below in Figure 4.2.2.a.

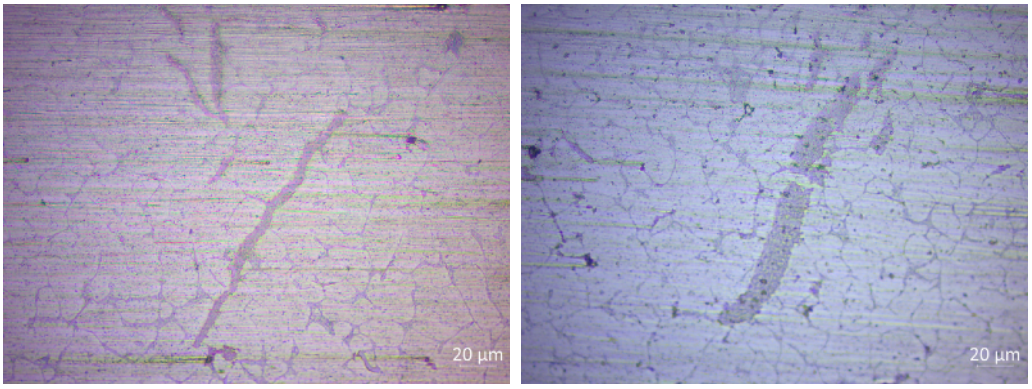

Figure 4.2.2.a TiB_2 secondary phase in the weld zone for (a) AA 6061 weld, (b) AA 5083 weld

For the AA 2024 & 5083 with 4943 1.25% volume TiB_2 sample, TiB_2 clusters of about 76 µm in length were observed. In general, these clusters were smaller than the clusters observed with 4943 1% volume TiB_2 filler, which reached 129 µm in length. In addition, secondary phase was noticeably more distributed in the welded state with smaller aluminum grains when compared to the casted material in Figure 4.1.d. OM images from the welded dissimilar samples can be seen on the next page in Figure 4.2.2.b.

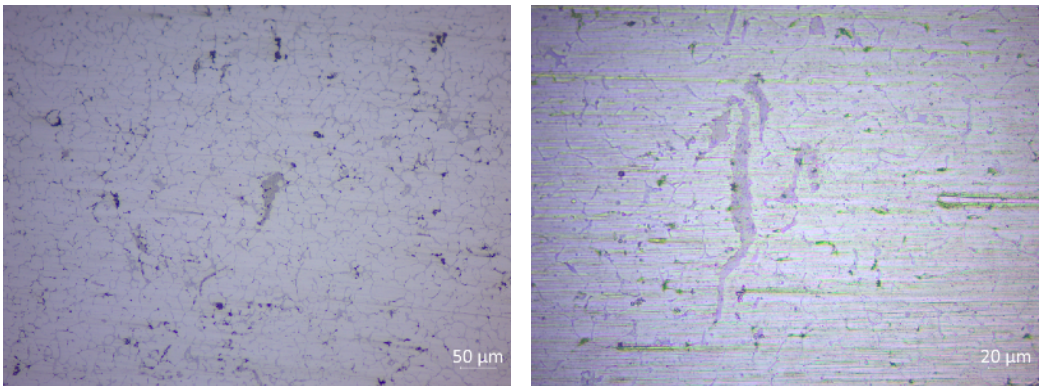

Figure 4.2.2.b TiB_2 clusters observed in (a) 4943 1.25% TiB_2 filler and (b) 4943 1% TiB_2 filler

In general, samples showed excellent porosity characteristics with little to no hydrogen voids in the weld zone. Secondary phase in the weld zone for reference welds had a more even distribution than that of the TiB_2 nanocomposite filler welds, due to TiB_2 nanoparticles populating secondary phase in the nano composite weld zone. A side-by-side comparison can be seen below in Figure 4.2.2.c for the AA 6061 & 6061 weld zone.

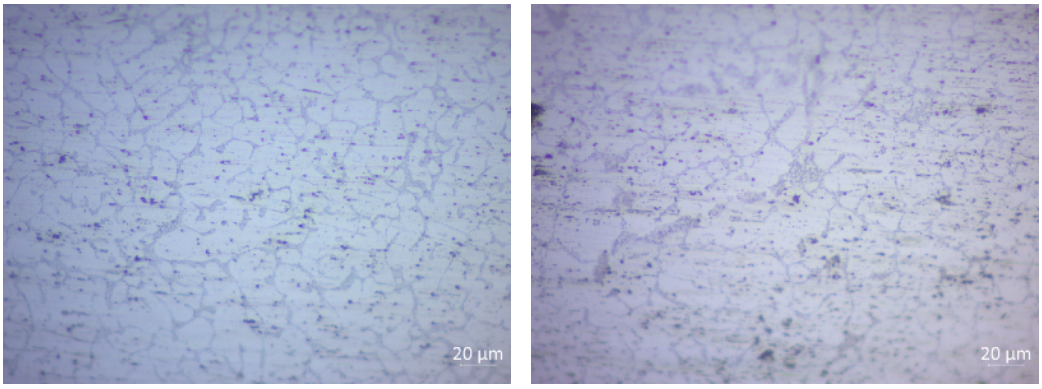

Figure 4.2.2.c AA 6061 & 6061 weld zone for (a) AA 4943 reference filler weld, (b) AA 4943 1.25% volume TiB2 filler weld

These clusters of TiB_2 may prove to be problematic for the strength of the welds as they provide a surface for cracking to occur. Additional manufacturing methods such as extrusion of the welding wire can facilitate more even distribution of the TiB_2 nanoparticles.

Section 4.2.2.1 Microstructure

For the 7075 & 7075 weld, Weck's reagent was used to determine grain boundaries under polarized light. One cycle of 15 seconds immersion in Weck's was used for the 7075 & 7075 sample with 4943 1% volume TiB_2 filler, while one cycle of 15 seconds and one cycle of 5 seconds was used for the 7075 & 7075 sample with 4943 reference filler. The results of this etching process along the fusion zone can be seen below in Figure 4.2.2.1.a.

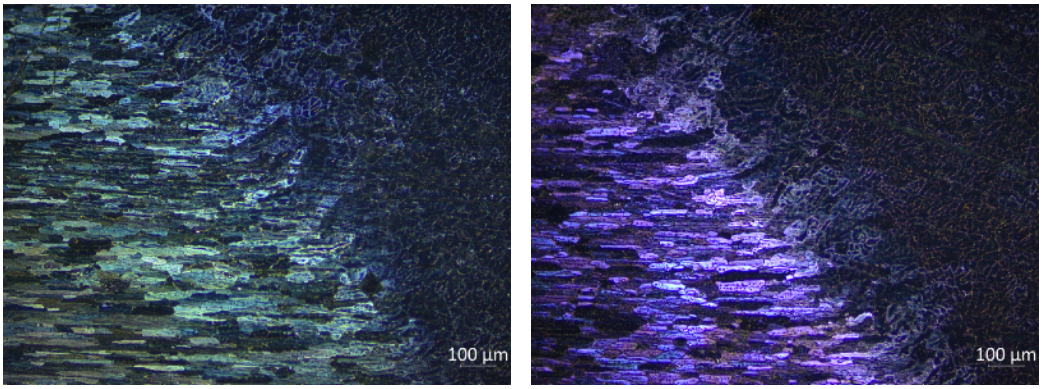

Figure 4.2.2.1.a AA 7075 & 7075 sample with (a) 4943 1%v TiB_2 filler and (b) 4943 reference filler

As can be seen, Weck's reagent works well with AA 7075 for determining grain structure under polarized light. However, while general grain structure is revealed in the 4943 filler material, this area remains mostly dark under polarized light. This makes it unsuitable for determining microstructure size in the weld zone, as the boundaries between phases cannot be determined.

Similar results were seen for the dissimilar welds of AA 2024 & 5083. For these welds, grain structure under polarized light could only be seen in the AA 2024 base material, or one side of the weld. This process used 15 seconds of immersion in Weck's reagent for both the 4943 1.25% volume TiB_2 filler weld and the 4943 reference weld. Results from this etching process can be seen on the next page in Figure 4.2.2.1.b.

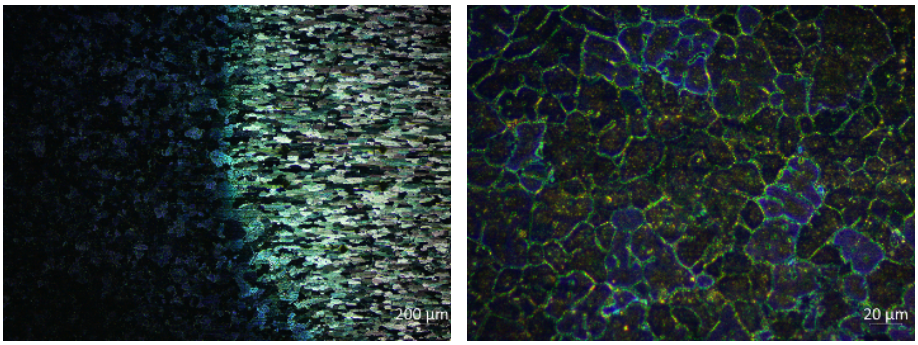

Figure 4.2.2.1.b AA 2024 & 5083 sample with (a) 4943 1.25%v TiB_2 filler and (b) 4943 reference filler

For the AA 2024 & 2024 weld, Weck's reagent successfully etched the AA 2024 base material; however, the nanocomposite AA 4943 filler material remained mostly dark under polarized light as with previous samples. The results of this can be seen below in Figure 4.2.2.1.c.

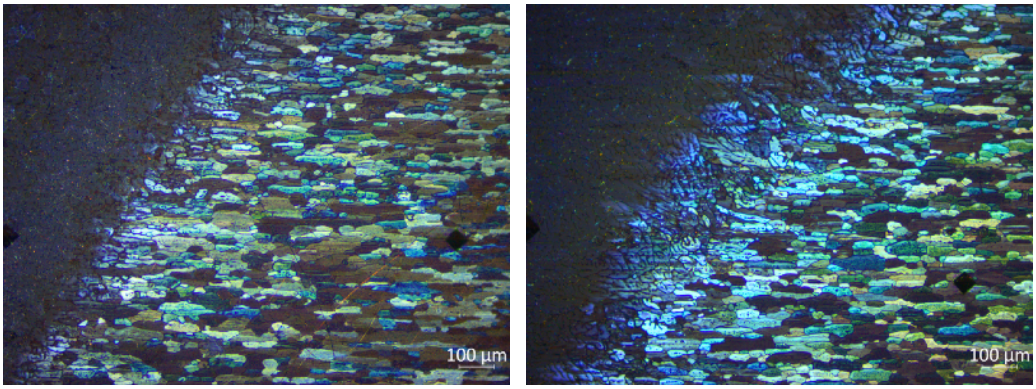

Figure 4.2.2.1.c AA 2024 & 2024 sample (a) within fusion zone and (b) within weld zone

Weck's reagent etching was also attempted for the 6061 & 6061 weld. While some grain structure in the 6061 base material was revealed under polarized light after 60 seconds of immersion in Weck's (four 15 second cycles), this resulted in overetching and pitting on the surface of the material. In addition, the AA 4943 filler material remained mostly dark and only general grain boundaries were revealed.

Electroetching with Barker's reagent was used on the dissimilar AA 2024 & 5083 weld with 25 seconds of immersion and the weld sample as the anode under 0.1 A of current. Similarly to etching with Weck's reagent, the AA 4943 filler material remained dark under polarized light and only general structure was revealed. Some polarization was seen on the AA 2024 base material; however, the 25 second cycle resulted in pitting on the material. The results of this process can be seen below in Figure 4.2.2.1.d.

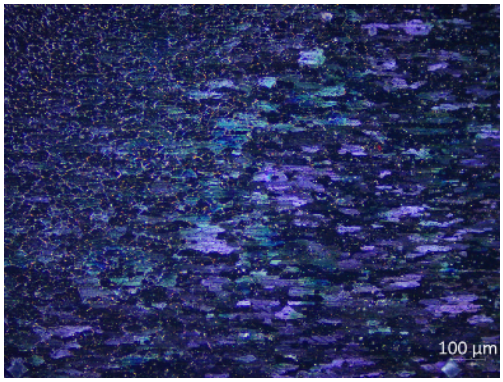

Figure 4.2.2.1.d Dissimilar weld with 25 seconds of electroetching in Barker's reagent

Per ASTM E407, the recommended etchant for 4xxx series aluminum alloys is a solution of 2 mL HF, 3 mL HCl, 5 mL HNO_3, and 190 mL deionized water[50]. This etchant was made using solutions of 38% HCl by weight, 30% HF by weight, and 70% HNO_3 by weight. After combining, the etchant was allowed to rest for five minutes as its color slowly changed to a yellow tint. After five minutes, samples were immersed in the etchant for 15 seconds each. This process revealed the general structure for the AA 4943 and AA 2024; however, AA 6061 and AA 5083 was not affected. Results from this process for the AA 6061 & 6061 nanocomposite and reference filler welds, as well as the AA 2024 & 5083 nanocomposite and reference filler welds, can be seen on the next page in Figure 4.2.2.1.e.

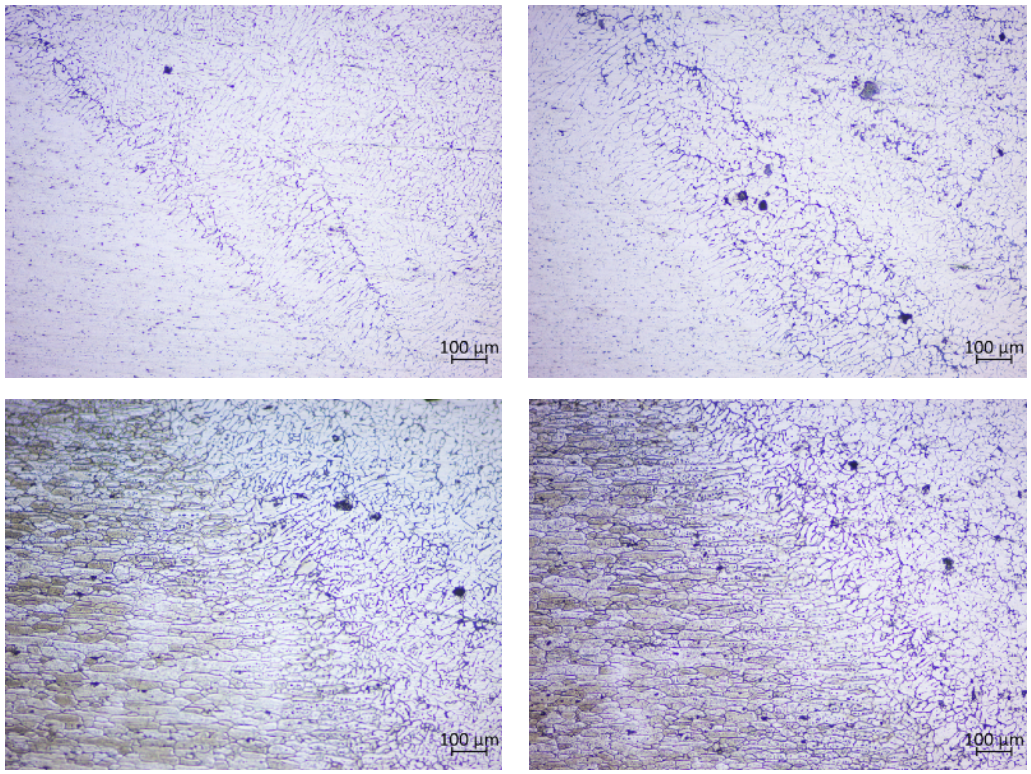

Figure 4.2.2.1.e Fusion zone of samples after etching (a) AA 6061 & 6061 with 4943 reference filler, (b) AA 6061 & 6061 with 4943 nanocomposite filler, (c) AA 2024 & 5083 with 4943 reference filler, (d) AA 2024 & 5083 with 4943 nanocomposite filler

While this process revealed the general structure of the samples, grain boundaries under polarized light remained limited. The results of polarized light on samples (c) and (d) shown in Figure 4.2.2.1.e is shown below in Figure 4.2.2.1.f.

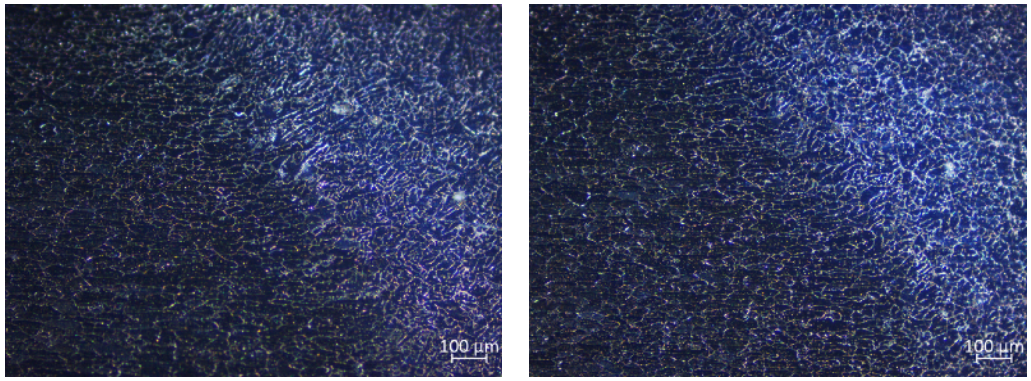

Figure 4.2.2.1.f Fusion zone of samples after etching under polarized light (a) AA 2024 & 5083 with 4943 reference filler, (b) AA 2024 & 5083 with 4943 nanocomposite filler

Despite restricted grain boundaries under polarized light, this etching process was used to determine the microstructure in the weld zone for the AA 4943 filer material. With the grain boundaries etched by the HF-HCl-HNO_3 solution, the size of grains were determined for the AA 6061 & 6061 welds with both AA 4943 reference filler and AA 4943 1.25% volume TiB_2 filler. Diagonal lines were sketched on the optical microscope images of the etched material, with the scale of the image facilitating determination of grain size based on number of boundaries crossed by the lines. For the AA 4943 nanocomposite filler sample, a grain size of 15.8 ± 0.75 μm was determined; for the AA 4943 reference filler sample, a grain size of 14.7 ± 1.3 μm. While there is room for error as polarized light was not used to determine grain boundaries, these results show limitations of using TiB_2 nanoparticles in AA 4943, particularly with AA 6061 base material.

Section 4.2.3 Tensile testing

Tensile testing was completed in order to confirm results shown with microhardness testing for the AA 6061 & 6061 and AA 2024 & 5083 welds. These welds were of most interest due to slight improvements in microhardness shown with AA 4943 nanocomposite filler. Results for the AA 6061 & 6061 weld show the weld with AA 4943 nanocomposite filler failing before the weld with AA 4943 reference filler. A summary of the results can be seen on the next page in Figure 4.2.3.1

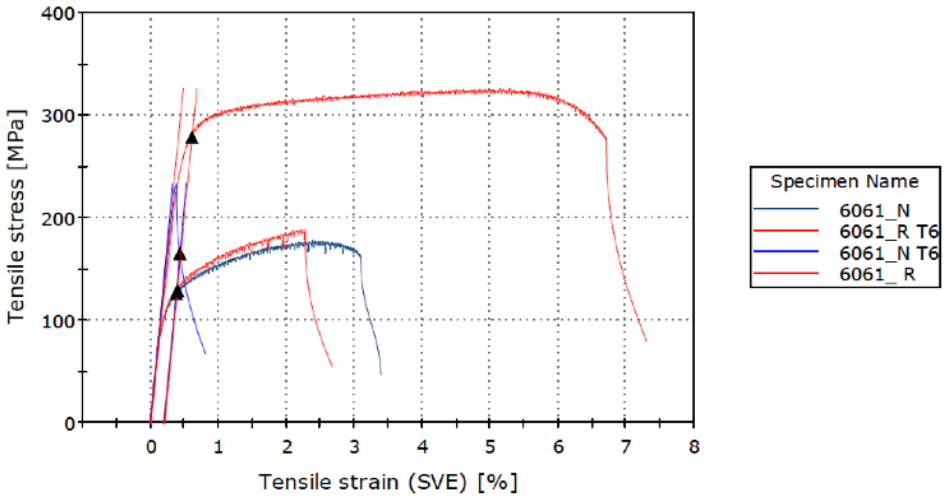

Specimen label	Maximum Load	Tensile stress at Maximum Load	Tensile stress at Yield (0.2%)
	(N)	(MPa)	(MPa)
6061_N	4396.79	178.01	126.64
6061_R T6	8884.19	325.43	278.47
6061_N T6	6079.04	233.81	165.44
6061_ R	6625.14	188.75	129.33

Figure 4.2.3.1 Stress-strain curve for AA 6061 & 6061 welds

This result, which confirms the microstructure results from Section 4.2.2.1, could be due to many factors including impurities in the weld zone of the nanocomposite filler that are not present in the weld fabricated with extruded AA 4943 reference material, such as oxidation impurities in the casted filler material. The most likely reason for the early failure of the nanocomposite samples is the clustering of the TiB_2 nanoparticles, which hinder the ductility of the samples and cause early failure. These clusters may also be prohibiting the uniform dispersion of precipitates in the heat treated samples. The AA 4943 reference filler sample noticeably failed in the AA 6061 base material, in contrast to the AA 4943 nanocomposite filler sample failing in the weld zone. These samples can be seen on the next page in Figure 4.2.3.2.

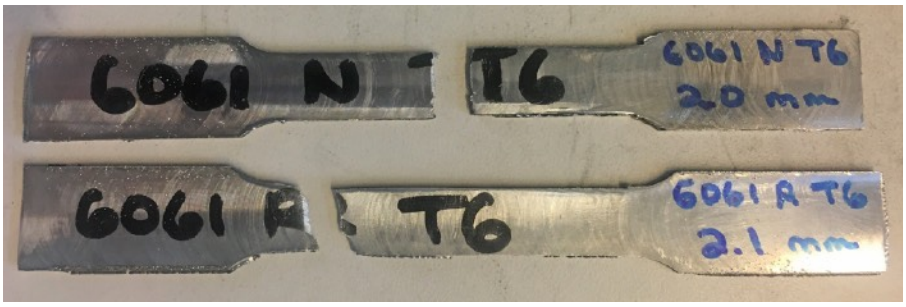

Figure 4.2.3.2 Fractured tensile bars for AA 6061 & 6061 samples

Despite the failure above, results of tensile testing may not "totally represent the strength and ductiity properties of the entire end product or its in-service behavior in different environments"[25]. Any additional tensile tests would offer confirmation of these results, particularly with different weldments in different environmental conditions.

IV. Summary

Nanocomposites have shown great promise in overcoming problems associated with GTA aluminum welding, including solidification cracking, liquation cracking, reduced strength due to heat input, and porosity. In particular, Sokoluk et al. demonstrated that through the addition of TiC nanoparticles in filler material for AA 7075 welds, solidification cracking typically associated with welding high strength aluminum alloys can be avoided[2].

The idea of using nanocomposite filler to overcome these problems and enhance the mechanical properties of aluminum welds fabricated with GTAW can be extrapolated to other combinations of aluminum alloys. For this thesis, a very popular welding filler material, AA 4943, was fabricated with TiB_2 nanoparticles to determine the effects of the nanomaterial on aluminum welds. Tests were completed for microhardness, microstructure, and tensile strength to determine these effects and whether ductility and tensile strength enhancements were achieved.

While the aluminum alloy welds with AA 4943 nanocomposite material showed no signs of cracking or porosity, enhancements to strength and ductility were limited or nonexistent. Minor improvements to microhardness were seen in the AA 6061 & 6061 weld using AA 4943 nanocomposite filler; however, this improvement has not been confirmed through tensile testing. In addition, refinements to grain boundaries were not seen for these samples, which further supports the idea that TiB_2 is not an effective reinforcement in the AA 4943 aluminum matrix.

There are many possible explanations for the lack of mechanical enhancements seen with adding TiB_2 nanoparticles to the AA 4943 filler material, including possible impurities in the weld bead originating from the casted sample, difference in amount of nanomaterial between samples that were tested, and sample-specific problems such as the extensive amount of alloying elements in AA 7075 which may not be receptive to the nanocomposite AA 4943

matrix. However, the most likely reason is the clustering of the TiB_2 nanoparticles, which hinders the ductility of the filler material and provides a brittle fracture surface. In addition, these clusters may be hindering the fluidity of the AA 4943, which is typically very fluid from the silicon in the alloy; this increases the probability of solidification cracking around the weld zone and decreased ultimate tensile strength.

TiC remains the preferred nanomaterial for welding filler nanocomposite due to its uniform distribution and superior refinement of the aluminum alloy microstructure. The benefit of adding nanomaterial to AA 4943, an alloy specifically designed for welding aluminum alloys such as AA 6061, remains questionable as TiC reacts with silicon and TiB_2 clusters in the AA 4943 matrix. Other nanomaterials may show more promise as reinforcement for welds fabricated with AA 4943 filler material.

V. Future Work

Many more steps can be taken to further studies of nanocomposite filler welds, specifically for AA 4943 filler wire. Etching for AA 4943 needs improvement to obtain more accurate grain boundaries under polarized light. With the given methods, including Weck's reagent, electroetching with Barker's reagent, and etching with an HF-HCl-HNO_3 solution, only a general structure can be revealed.

There is still potential for TiB_2 to enhance properties of AA 4943 filler welds with better nanoparticle distribution — which can be achieved through other fabrication methods, such as extrusion. Extruding nanocomposite AA 4943 filler material into wire may help solve the clustering issue shown with TiB_2 nanoparticles by breaking the clusters in different lengths of wire. Also, welding parameters can be changed to see if results differ with varying parameters. High quality, repeatable welds are needed in order to confirm the results shown with nanocomposite AA 4943 filler material.

Characterization tests, including microhardness and tensile testing, can also be repeated to obtain a more accurate portrayal of the effect of nanomaterial in AA 4943 filler welds. This thesis study primarily focused on the AA 6061 & 6061 weld, due to the widely accepted applicability of AA 4943 filler material with this base material. However, the other welds shown in the microhardness study in section 4.2.1, including AA 7075 & 7075 and AA 2024 & 2024, can be further studied for microstructure and tensile strength to determine applicability of AA 4943 nanocomposite filler to these aluminum alloys.

Other methods of aluminum welding, including friction stir welding and laser welding, can be looked into as a means to enhance the properties of commonly welded aluminum alloys. These methods avoid the massive heat input over a large area seen with GTAW, which causes a loss of strength in the base material.

VI. Appendices

Appendix 1 ASTM etchants for metals and alloys

Etchant	Composition	Procedure
1	1 mL HF 200 mL water	(a) Swab with cotton for 15 s. (b) Alternately immerse and polish several minutes. (c) Immerse 3–5 s. (d) Immerse 10–120 s.
2	3 mL HF 100 mL water	(a) Swab 10 s to reveal general structure. (b) Immerse 15 min, wash 10 min in water to form film with hatching which varies with grain orientation.
3	2 mL HF 3 mL HCl 5 mL HNO_3 190 mL water	(a) Immerse 10–20 s Wash in stream of warm water. Reveals general structure. (b) Dilute with 4 parts water-colors constituents—mix fresh.
4	24 mL H_3PO_4 50 mL Carbitol (diethylene glycol monoethyl ether) 4 g boric acid	Electrolytic: Use carbon cathode raising d-c voltage from 0–30 V in 30 s. Total etching time 3 min with agitation. Wash and cool. Repeat if necessary.
5	5 g HBF_4 200 mL water	Electrolytic: Use Al, Pb, or stainless steel cathode. Anodize 1–3 min, 20–45 V d-c. At 30 V, etch for 1 min.
6	25 mL HNO_3 75 mL water	Immerse 40 s at 70°C (160°F). Rinse in cold water.
7	10–20 mL H_2SO_4 80 mL water	Immerse 30 s at 70°C (160°F). Rinse in cold water.
8	10 mL H_3PO_4 90 mL water	(a) Immerse 1–3 min at 50°C (120°F). (b) Electrolytic at 1–8 V for 5–10 s.
222	8 g Na_2SO_4 100 mL water	(a) Few seconds to 1 minute. (b) Pre-etch 2 s in No. 74, rinse, and etch 20 s.

VII. References

[1] Anderson, T. (2013). A New Development in Aluminum Welding Wire: Alloy 4943. Welding journal, 92(7), 32-37.

[2] Sokoluk, M., Cao, C., Pan, S., & Li, X. (2019). Nanoparticle-enabled phase control for arc welding of unweldable aluminum alloy 7075. Nature communications, 10(1), 98.

[3] Pujari, K S, and Dr D V Patil. "A Review on GTAW Technique for High Strength Aluminium Alloys (AA 7xxx Series)." International Journal of Engineering Research 2, no. 8 (2013): 14.

[4] Joost, W. J. Reducing vehicle weight and improving U.S. energy efficiency using integrated computational materials engineering. JOM 64, 1032–1038 (2012).

[5] Callister. W.D, JR. (2007). Materials Science and Engineering: An Introduction. 7th edition. John Wiley & Sons, Inc.

[6] Aluminum 5083-H116; 5083-H321. Retrieved December 10, 2019, from http:// asm.matweb.com/search/SpecificMaterial.asp?bassnum=MA5083H116.

[7] Balasubramanian, V., Ravisankar, V., & Reddy, G. M. (2007). Effect of pulsed current and post weld aging treatment on tensile properties of argon arc welded high strength aluminium alloy. Materials Science and Engineering: A, 459(1-2), 19-34.

[8] Welder Portal (2018, August 28). What Is the Difference Between AC and DC Welding? Retrieved from https://welderportal.com/what-is-the-difference-between-ac-and-dc-welding/.

[9] Biradar, N. S. (2016). Effect of transverse mechanical arc oscillation on hot cracking (solidification & liquation) and weld metal properties of AA2014 T6 TIG welds. AIMS Materials Science, 3(4), 1544-1560.

[10] Pires, J. N., Loureiro, A., & Bölmsjo, G. (2006). Welding robots: technology, system issues and application. Springer Science & Business Media.

[11] Fadaeifard, F., Matori, K. A., Garavi, F., Al-Falahi, M., & Sarrigani, G. V. (2016). Effect of post weld heat treatment on microstructure and mechanical properties of gas tungsten arc welded AA6061-T6 alloy. Transactions of Nonferrous Metals Society of China, 26(12), 3102-3114.

[12] Kou, S. (2003). Solidification and liquation cracking issues in welding. Jom, 55(6), 37-42.

[13] Wu, Y. E., & Wang, Y. T. (2010). Enhanced SCC resistance of AA7005 welds with appropriate filler metal and post-welding heat treatment. Theoretical and Applied Fracture Mechanics, 54(1), 19-26.

[14] Aluminum Workshop: The best filler wire for welding 6061-T6 aluminum. Retrieved from https://www.thefabricator.com/thewelder/article/aluminumwelding/which-filler-wire-is-best-for-welding-6061-t6-aluminum-5356-or-4043r.

[15] Rajan, R., Kah, P., Mvola, B., & Martikainen, J. (2016). Trends in Aluminum Alloy Development and Their Joining Methods. Reviews on Advanced Materials Science, 44(4).

[16] Yu, H., Xu, Y., Song, J., Pu, J., Zhao, X., & Yao, G. (2015). On-line monitor of hydrogen porosity based on arc spectral information in Al–Mg alloy pulsed gas tungsten arc welding. Optics & Laser Technology, 70, 30-38.

[17] Zhou, W. (1999). Problems in welding of high strength aluminium alloys. Singapore Welding Society Newsletter, 1.

[18] Poolperm, P., & Nakkiew, W. (2016). Effect of porosity on residual stress of 2024-aluminum GTAW specimen. In Materials Science Forum (Vol. 872, pp. 28-32). Trans Tech Publications.

[19] Rao, K. P., Ramanaiah, N., & Viswanathan, N. (2008). Partially melted zone cracking in AA6061 welds. Materials & Design, 29(1), 179-186.

[20] Kou, S., & Le, Y. (1985). Improving weld quality by low-frequency arc oscillation. Welding Journal, 64(3), 51-55.

[21] Dewan, M. W., Wahab, M. A., & Okeil, A. M. (2015). Influence of weld defects and postweld heat treatment of gas tungsten arc-welded AA-6061-T651 aluminum alloy. Journal of Manufacturing Science and Engineering, 137(5), 051027.

[22] Dewan, M. W., Liang, J., Wahab, M. A., & Okeil, A. M. (2012, November). Effects of residual stresses and the post weld heat treatments of TIG welded aluminum alloy AA6061-T651. In ASME 2012 International Mechanical Engineering Congress and Exposition (pp. 811-820). American Society of Mechanical Engineers.

[23] ASM International. Handbook Committee. (1991). ASM handbook: Heat treating (Vol. 4). Asm Intl.

[24] Norman, A. F., S. S. Birley, and P. B. Prangnell. "Development of New High Strength Al – Sc Filler Wires for Fusion Welding 7000 Series Aluminium Aerospace Alloys." Science and Technology of Welding and Joining 8, no. 4 (August 2003): 235–45. https://doi.org/10.1179/136217103225010989.

[25] Norman, A. F., Birley, S. S., & Prangnell, P. B. (2003). Development of new high strength Al–Sc filler wires for fusion welding 7000 series aluminium aerospace alloys. Science and technology of welding and joining, 8(4), 235-245.

[26] Washington Alloy Company. (2018). 4043 Aluminum Welding Wire. Retrieved November 9, 2019, from https://weldingwire.com/Images/Interior/documentlibrary/4043.pdf.

[27] Washington Alloy Company. (2018). 4943 Aluminum Welding Wire. Retrieved October 1, 2019, from https://weldingwire.com/Images/Interior/product tech sheets/4943.pdf.

[28] Washington Alloy Company. (2018). 4356 Aluminum Welding Wire. Retrieved November 9, 2019, from https://weldingwire.com/Images/Interior/documentlibrary/5356_aluminum_welding_wire.pdf.

[29] Hobart®MaxalMig® /MaxalTig® 4943. (2016). Retrieved December 10, 2019, from https://www.hobartbrothers.com/downloads/maxalmig_maxalti_quQnJ.pdf.

[30] Huang, C., & Kou, S. (2003). Liquation cracking in partial-penetration aluminum welds: Effect of penetration oscillation and backfilling. WELDING JOURNAL-NEW YORK-, 82(7), 184-S.

[31] M. Ishak, K. Maekawa and K. Yamasaki // Materials Science and Engineering: A 536 (2012) 143.

[32] A.M. Orishich, A.G. Malikov and A.N. Cherepanov // Physics Procedia 56 (2014) 507.

[33] D.Wolfgang and A. Dorfen, Introduction of nanoparticles, United States of America Patent 8,240,544 B2, 14 August 2012.

[34] S. R. Bakshi and A. B. Agarwal. Carbon 49 (2011) 533.

[35] R. Pérez-Bustamante, F. Pérez-Bustamante, I. Estrada-Guel, L. Licea-Jiménez, M. Miki-Yoshida and R. Martinez-Sánchez. Materials Characterization 75 (2013) 13.

[36] Vimalraj, Cyril, Paul Kah, Belinga Mvola, and Jukka Martikainen. "Effect of Nanomaterial Addition Using GMAW and GTAW Processes," n.d., 13.

[37] M. Fattahi, N. Nabhani, E. Rashidkhani, Y. Fattahi, S. Akhavan and N. Arabian // Micron 54-55 (2013) 28.

[38] Fattahi, M., Mohammady, M., Sajjadi, N., Honarmand, M., Fattahi, Y., & Akhavan, S. (2015). Effect of TiC nanoparticles on the microstructure and mechanical properties of gas tungsten arc welded aluminum joints. Journal of materials processing technology, 217, 21-29.

[39] Hansen, N. (2004). Hall–Petch relation and boundary strengthening. Scripta Materialia, 51(8), 801-806.

[40] Zhang, Z., & Chen, D. L. (2008). Contribution of Orowan strengthening effect in particulate-reinforced metal matrix nanocomposites. Materials Science and Engineering: A, 483, 148-152.

[41] Javadi, A., Cao, C., & Li, X. (2017). Manufacturing of Al-TiB2 Nanocomposites by Flux-Assisted Liquid State Processing. Procedia Manufacturing, 10, 531-535.

[42] Sabetghadam-Isfahani, A., Zalaghi, H., Hashempour, S., Fattahi, M., Amirkhanlou, S., & Fattahi, Y. (2016). Fabrication and properties of ZrO2/AZ31 nanocomposite fillers of gas tungsten arc welding by accumulative roll bonding. Archives of Civil and Mechanical Engineering, 16(3), 397-402.

[43] Kennedy, A. R., Karantzalis, A. E., & Wyatt, S. M. (1999). The microstructure and mechanical properties of TiC and TiB2-reinforced cast metal matrix composites. Journal of materials science, 34(5), 933-940.

[44] Ding, H. M., & Liu, X. F. (2011). Influence of Si on stability of TiC in Al melts. Transactions of Nonferrous Metals Society of China, 21(7), 1465-1472.

[45] Mohammadtaheri, M. (2012). A new metallographic technique for revealing grain boundaries in aluminum alloys. Metallography, Microstructure, and Analysis, 1(5), 224-226.

[46] Roy, R. K., & Das, S. (2006). New combination of polishing and etching technique for revealing grain structure of an annealed aluminum (AA1235) alloy. Journal of materials science, 41(1), 289-292.

[47] Gao, L., Harada, Y., & Kumai, S. (2015). Microstructural characterization of aluminum alloys using Weck's reagent, part I: Applications. Materials Characterization, 107, 426-433.

[48] Weck, E., & Leistner, E. (1986). Metallographic instructions for colour etching by immersion, part iii: non-ferrous metals, cemented carbides and ferrous metals, nickel-base and cobalt-base alloys. DVS GmbH, Düsseldorf.

[49] B. Suárez-Peña, J. Asensio-Lozano, G.F. Vander-Voort, Colour metallography in commercial Al–Si alloys. Optimization of the microstructural characterization techniques in light optical microscopy, Rev. Met. 46 (2010) 469–476.

[50] ASTM E407-07. (2015). Standard practice for microetching metals and alloys.

[51] ASTM, E. 9. (2001). Standard test methods for tension testing of metallic materials. Annual book of ASTM standards. ASTM.

[52] Aluminum 6061-T6; 6061-T651. Retrieved December 10, 2019, from http://asm.matweb.com/search/SpecificMaterial.asp?bassnum=MA6061T6.